5. Seasonal Volatility Dependence of Ambient Particle Phase Amines

i. Introduction

Atmospheric aerosol particles play a major role in impacting global climate, regional air pollution, and human health (174). Organic carbon (OC) can comprise up to 50% of the total fine aerosol mass at continental midlatitudes (174), and in some areas, such as the eastern Los Angeles (LA) basin, secondary organic aerosol (SOA) can also represent a significant fraction of the total organic aerosol mass (175). During atmospheric transport, particles undergo heterogeneous reactions with trace gases as well as gas-to-particle partitioning of semivolatile species, causing changes in particle size, structure, and chemical composition (174). Understanding the partitioning of organic carbon species between the gas and particle phases remains one of the major challenges in predicting aerosol chemistry in regional and global atmospheric chemical transport models (174). In particular, semivolatile organic nitrogen species, suggested to be a significant portion of the OC aerosol mass (176), are not well understood with regard to gas-particle partitioning. The atmospheric lifetimes of organic nitrogen species are dependent on the distributions between the gas and particle phases for the different species, which in turn determine their role in the global nitrogen cycle (177). One class of semivolatile organic nitrogen species, alkylamines, is emitted from many of the same sources as ammonia, an abundant atmospheric species which has been extensively studied. In particular, a major source of nitrogen species is animal husbandry, where amine concentrations represent up to 23% of those measured for ammonia (178,179). Amines have also been identified in urban and rural atmospheres in both the gas and particle phases, including within fog and rainwater (39,180,181). Recent measurements show fine particulate amine concentrations of 0.5-6 $\mu g/m^3$ (up to ~20% of the organic matter mass) during winter inversions in Utah (182).

Amines can undergo oxidation by OH, O_3, and/or NO_3 to form amides, nitramines, and imines, which can also partition to the particle phase (176,178,182). Once in the particle phase, amines can undergo further reactions to form high-molecular-weight compounds (176,182,183). In addition, gas-phase aliphatic amines, which are stronger bases than ammonia, compete to form salts through the following reactions with nitric acid (HNO_3) and sulfuric acid (H_2SO_4), leading to secondary aerosol formation (39,176).

$$NR_{3(g)} + HNO_{3(g)} \underset{\leftarrow}{\overset{\rightarrow}{}} HNR_3NO_{3(s)} \xrightarrow{T,RH,pH} HNR_3^{+}{}_{(aq)} + NO_3^{-}{}_{(aq)} \qquad (1)$$

$$2NR_{3(g)} + H_2SO_{4(g)} \underset{\leftarrow}{\overset{\rightarrow}{}} (HNR_3)_2SO_{4(s)} \xrightarrow{T,RH,pH} 2(HNR_3)^{+}{}_{(aq)} + SO_4^{2-}{}_{(aq)} \qquad (2)$$

Particle phase amines associated with sulfate and nitrate have been observed in both chamber (39,176) and field measurements (184). Notably, chamber experiments by Murphy et al. (176) demonstrated the stability of nitrate salts of trimethylamine and triethylamine in the particle phase, even at very low relative humidity (RH <10%). However, one hypothesis suggests that if relative humidity is high and water is present in the particles, the aminium salts will dissolve into their ionic forms, shifting the equilibrium of the gas-phase amines toward the particle phase (39), potentially yielding

greater particle phase amine mass than predicted by Murphy et al. (176). As such, the gas/particle partitioning model described by Pankow (185) assumes that amines, as strong bases, are only volatile when present in their neutral, non-salt forms. In addition, due to low vapor pressures, organic acids may also form salts with amines, as suggested by measurements of atmospheric nanoparticles (186) and thermodynamic calculations (187).

To study the volatility behavior of alkylamine species within aged ambient particles in Riverside, CA, an automated thermodenuder (TD) was coupled to a real-time, single-particle mass spectrometer to characterize the chemical composition of the remaining individual submicrometer ambient organic carbon-containing particles following heating. Using the TD, semivolatile species were vaporized at different temperatures, leaving behind particle cores that were compared to the unheated particle chemistry (188). Herein, the partitioning of amines associated with nitrate and sulfate as a function of temperature and particle acidity are examined for individual organic carbon particles internally mixed with nitrate, sulfate, and ammonium.

ii. Experimental

a. Ambient Measurements

Measurements of individual submicrometer ambient aerosol particles by aerosol time-of-flight mass spectrometry (ATOFMS) were conducted during the Study of Organic Aerosols in Riverside (SOAR, August and November 2005, http://cires.colorado.edu/jimenez-group/Field/Riverside05/). The sampling site at the University of California, Riverside campus was located about ~60 miles east of Los Angeles, CA. Ambient temperature and atmospheric water content measurements were made using a shielded Vaisala HMP 45AC temperature and RH probe. The ATOFMS results presented here focus on TD-conditioned aerosol chemistry measurements made on August 12, 2005 (SOAR-1) and November 2-13, 2005 (SOAR-2). August 12th was the only summer day during which TD-conditioned aerosol chemistry was measured; however, it was typical of the particle chemistries and sources observed during SOAR-1 (189). From July 30 to August 15, 2005, a strong diurnal pattern was observed for ozone, particle mass concentrations, and ambient meteorological conditions, as shown in Table 6 (189). On August 12th, the wind predominantly (~80% frequency) came from the west, crossing the LA basin en route to Riverside; during SOAR-2, westerly winds were observed ~50% of the sampling time, with winds from the southwest contributing ~45% of the time (189).

An automated valve-controlled TD system (190) was utilized in series with the ATOFMS. In the fall only, a nafion dryer was used to dry the particles before the TD. In addition to water, the drying process may have removed some of the neutral amines and ammonium nitrate from the particle phase. However, the non-volatile aminium salts would not have been removed. Thus, the drying during the fall is not expected to impact the aminium salt mass present at 230°C. With continuous aerosol flow through the TD (heated) and bypass line (unheated), the particles sampled by the ATOFMS switched between heated and unheated ambient aerosol every 10 min. The heated portion of the TD stepped through 8 temperature steps: 171, 230, 201, 171, 142, 113, 83, and 54 °C;

temperatures noted here refer to actual temperatures, rather than set-points (190). Since each portion of the schedule was maintained for 10 min, one full cycle took 160 min before repeating. An activated carbon diffusion denuder

	SOAR-1	
	July 30 - Aug. 15, 2005	**Aug. 12, 2005**
Ozone (ppb)	34.9 (33.3)	26.2 (26.0)
Relative humidity (%)	56.8 (19.2)	68.6 (18.5)
Ambient temperature (°C)	25.7 (5.3)	22.9 (4.6)
Wind speed (m/s)	0.9 (0.8)	0.9 (0.8)
Wind direction (deg.)	224 (66)	223 (62)
$PM_{2.5}$ mass concentrations (μm/m^3)	33 (13)	37 (18)
$PM_{1.0}$ agedOC-nitrate-sulfate particle type mass concentrations (μm/m^3)	6.1 (3.3)	7.0 (3.4)

Table 6: Averages and standard deviations of ozone, ambient meteorological conditions, $PM_{2.5}$ mass concentrations (measured at the California Air Resources Board Rubidoux site), and $PM_{1.0}$ agedOC-nitrate-sulfate particle type mass concentrations for July 30 – August 15, 2005 compared to August 12, 2005 (189).

prevented volatilized species from condensing back onto the particles. With a flow rate of 0.6 lpm, the residence time of the aerosol in the heating portion of the TD was approximately 9 s.

The ground-based prototype of the aircraft (A)-ATOFMS, described in detail in Chapter 2, was utilized to measure the vacuum aerodynamic diameter (d_{va}) and dual-polarity mass spectra of individual particles from ~70-1000 nm in real time. Particles were desorbed and ionized using 266 nm radiation from a Q-switched Nd:YAG laser; thus, one or two photon ionization would provide 4.7 or 9.4 eV, readily ionizing the alkylamines with lower ionization potentials (~7.5 eV) compared to most organic species (~8-12 eV) (NIOSH, 191). The use of lower laser powers can lead to decreased ion fragmentation (192); however, while a slightly lower average laser power was utilized in the fall (~0.6 mJ) compared to the summer (~0.95 mJ), the amine signature was not found to be impacted. Polystyrene latex spheres (PSLs) of known physical diameter from 95-1400 nm were used for the particle size calibration. Dual-polarity mass spectra were collected with the ATOFMS for 318,431 ambient particles on August 12, 2005 and 1,390,199 ambient particles from November 2-13, 2005. Data collection times were adjusted for delays in transport lines between the TD and ATOFMS, and data collected up to 20 seconds after the TD valve switch were eliminated to reduce error caused by possible aerosol mixing. Taking this delay into account, the mass spectra from 141,757 unheated and 119,888 heated particles were analyzed for August 12, and 717,705 unheated and 462,982 heated particles were analyzed for November 2-13.

For detailed analysis, single-particle mass spectra were imported into YAADA (www.yaada.org), a software toolkit for Matlab (The MathWorks, Inc.), for analysis. An adaptive resonance theory-based clustering method (ART-2a) (193) was then used to group single-particle mass spectra with a vigilance factor of 0.80, learning rate of 0.05, 20 iterations, and regrouping with a vigilance factor of 0.85. ART-2a classifies particles into separate clusters based on the presence and intensity of ion peaks in individual single-particle mass spectra. Peak identifications within this paper correspond to the most probable ions for a given *m/z* ratio. The ART-2a clusters resulting from the analysis of single SOAR unheated and heated particles (100-1000 nm) were classified into thirteen general particle types: aged organic carbon (mixed with ammonium, sulfate, and

nitrate, herein referred to as the aged OC particle type), aromatic, amine, ammonium-rich, elemental carbon-organic carbon (ECOC), inorganic-ECOC, elemental carbon (EC), vanadium, biomass, aged sea salt, dust, metals, and nitrate-sulfate particles with no positive ions (NoPos). The size-resolved chemistry of the unheated particles is shown in **Figure 35** for SOAR-1 (summer) and SOAR-2 (fall). It should be noted that the vast majority of unheated particles show evidence of organic carbon markers, nitrate, and sulfate due to aging during transport across the LA basin to Riverside (158). Detailed descriptions of mass spectral, size, and temporal patterns of the majority of the unheated SOAR ATOFMS particle types are described elsewhere (189). Herein, we focus on the aged OC (nitrate-sulfate) particle type, described below.

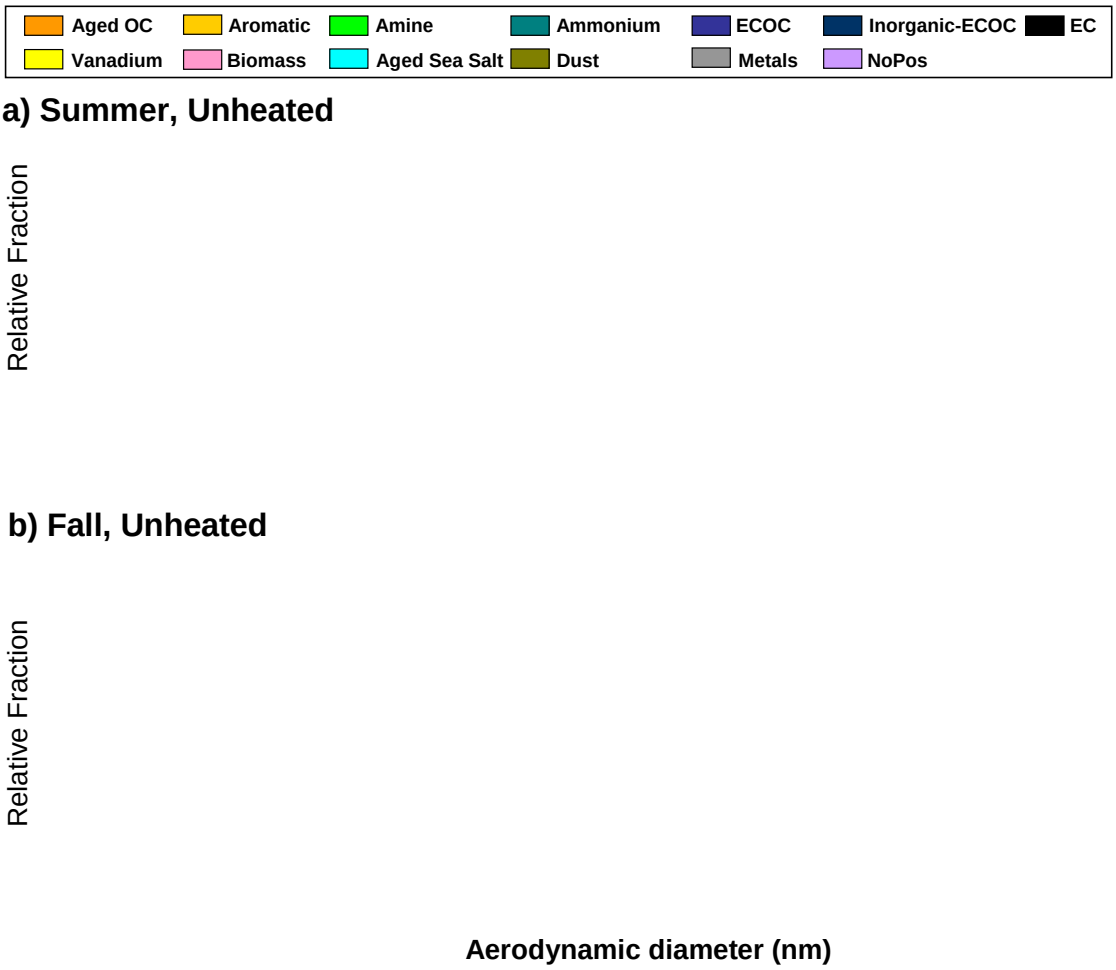

Figure 35: Size-resolved chemical composition of unheated particles during (a) SOAR-1 (summer) and (b) SOAR-2 (fall). Size resolution is 10 nm and 50 nm for the ranges of 100-350 nm and 350-1000 nm, respectively. The majority of the particles greater than ~150 nm show evidence of internally mixed organic carbon, ammonium, nitrate, and sulfate.

b. Amine Mass Calibration

To determine the mass of amines present in the submicrometer aged OC (nitrate-sulfate) particle type during SOAR, triethylamine vapor was coated onto PSLs, which serve as proxies for the SOAR OC particle matrix. A schematic of the experimental

setup is shown in **Figure 36**. An aqueous (milli-Q water) solution of 270 nm PSLs (Invitrogen Corp.) was atomized using filtered ambient air at a flow rate of 3.0 $L \cdot min^{-1}$. The PSLs were dried using two silica gel diffusion dryers and the flow subsequently split between exhaust (1.0 $L \cdot min^{-1}$) and a differential mobility analyzer (DMA, TSI, Inc., Model 3081, sample flow = 2.0 $L \cdot min^{-1}$, sheath flow = 5.0 $L \cdot min^{-1}$) to narrow the particle distribution. The size-selected PSLs were passed through a dilution chamber where supplemental filtered ambient air was added (0.2 $L \cdot min^{-1}$), followed by introduction into a glass mixing chamber (~ 20 L, residence time ~10 min). To initiate coating, gas phase precursors were introduced by placing liquid reservoirs directly within the reaction chamber; the headspace over these reservoirs acted as the vapor source. In the initial experiment, aiming to condense amine salts onto the PSL seed, two flasks each containing ~2mL of either TEA (Acros Organics, 99+%) or nitric acid (Sigma-Aldrich, 99.999+%) were quickly (<1 min) placed directly into the chamber. During this trial, extensive homogeneous nucleation was observed between TEA and nitric acid, overwhelming the PSL seeds (results not shown). To eliminate new particle formation, and partition TEA exclusively to PSLs, a second experiment was performed in which TEA only was coated onto PSLs. The chamber output flowed through two inline activated carbon denuders spiked with sodium carbonate and boric acid, respectively, to remove any gaseous reactants prior to parallel analysis by a scanning mobility particle

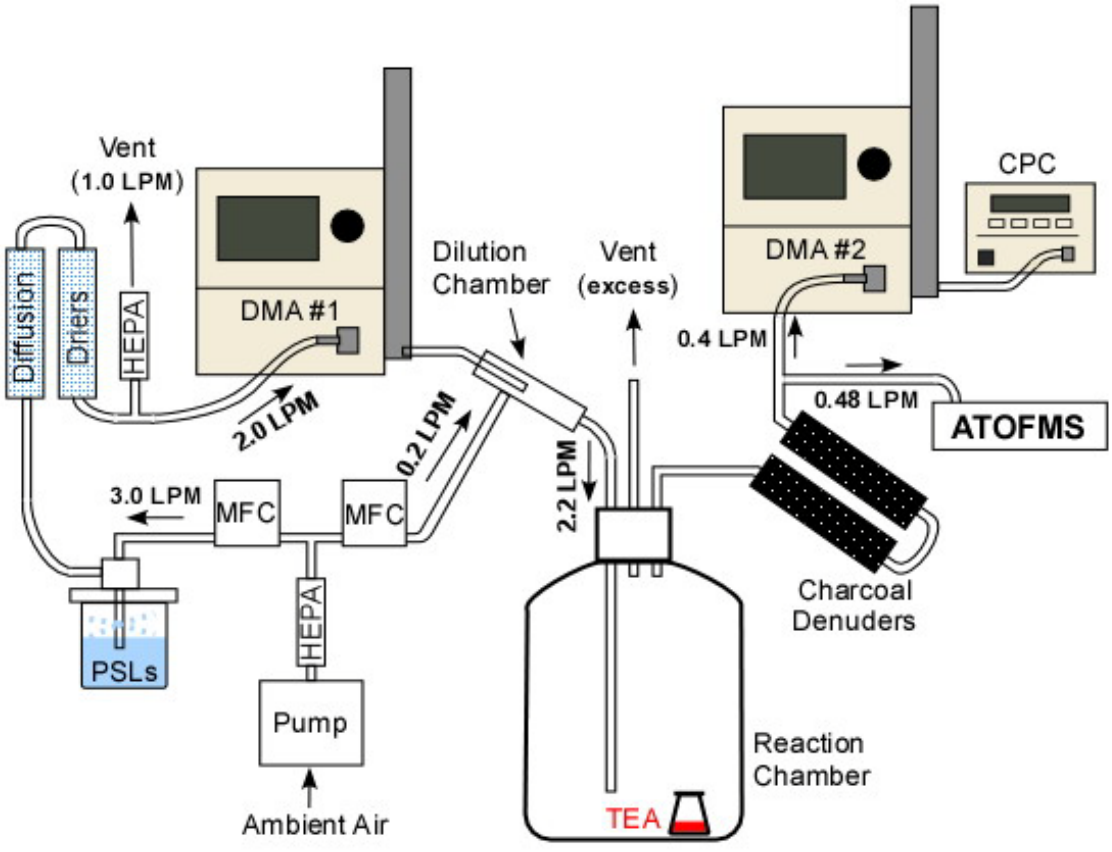

Figure 36: Amine mass calibration experimental set-up (MFC = mass flow controller; TEA = triethylamine; DMA = differential mobility analyzer; CPC = condensation particle counter; ATOFMS = aerosol time-of-flight mass spectrometer).

sizer (SMPS, TSI, Inc., DMA model 3081 – 0.4/4.0 LPM; CPC Model 3010) to monitor the particle size distribution and A-ATOFMS to obtain the single particle mass spectra and vacuum aerodynamic diameter (D_{va}). Background SMPS scans were obtained prior to addition of PSLs to confirm that the system was free of particle contamination; SMPS scans of uncoated PSLs were made to ensure a monodisperse seed aerosol distribution. Representative SMPS and ATOFMS size distributions of the uncoated and TEA-coated PSLs are shown in **Figure 37**.

The single particle mass spectra for uncoated and TEA-coated PSLs were imported into MatLab (The MathWorks, Inc.) for analysis following the methods described for treating the SOAR data. The dominant cluster of uncoated PSLs was identified as the PSL mass spectral signature (**Figure 38b**); only the TEA-coated aerosols exhibiting this specific PSL fingerprint (**Figure 38a**) were used in subsequent analysis to ensure a realistic comparison between coated and uncoated particles. In the TEA-coated PSLs, an ion peak representative of TEA is present at *m/z* 86($(C_2H_5)_2NCH_2^+$). It should be noted that the potential exists for differences in the UV absorption and ionization efficiency between protonated (salt bound) and neutral TEA, which would impact the calibration parameters of these two species; however these effects were not characterized in this study.

The polydisperse TEA coated particles were divided into 2 nm D_{va} size bins from 274-302 nm; subsequently bins from 274-280 nm and 292-302 nm were merged due to low ATOFMS particle counts. The average D_{va} and mass spectrum were calculated for each size bin as described below. A trend was observed whereby the *m/z* 86 peak area increased with decreasing D_{va}, as shown in **Figure 39**. However, the SMPS scans of

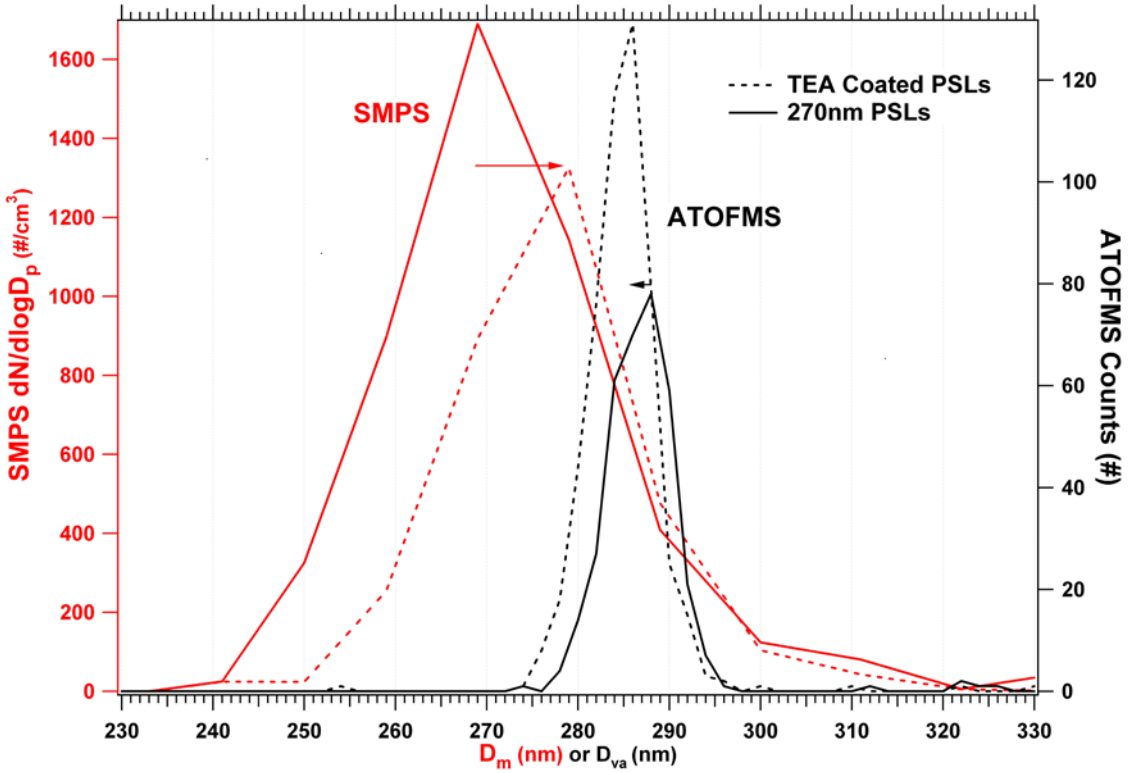

Figure 37: Size distributions of uncoated (solid) and TEA-coated (dashed) 270 nm PSLs. SMPS distributions of mobility diameter are shown in red; ATOFMS distributions of vacuum aerodynamic diameter are in black. The arrows indicate the shifts of the respective distributions.

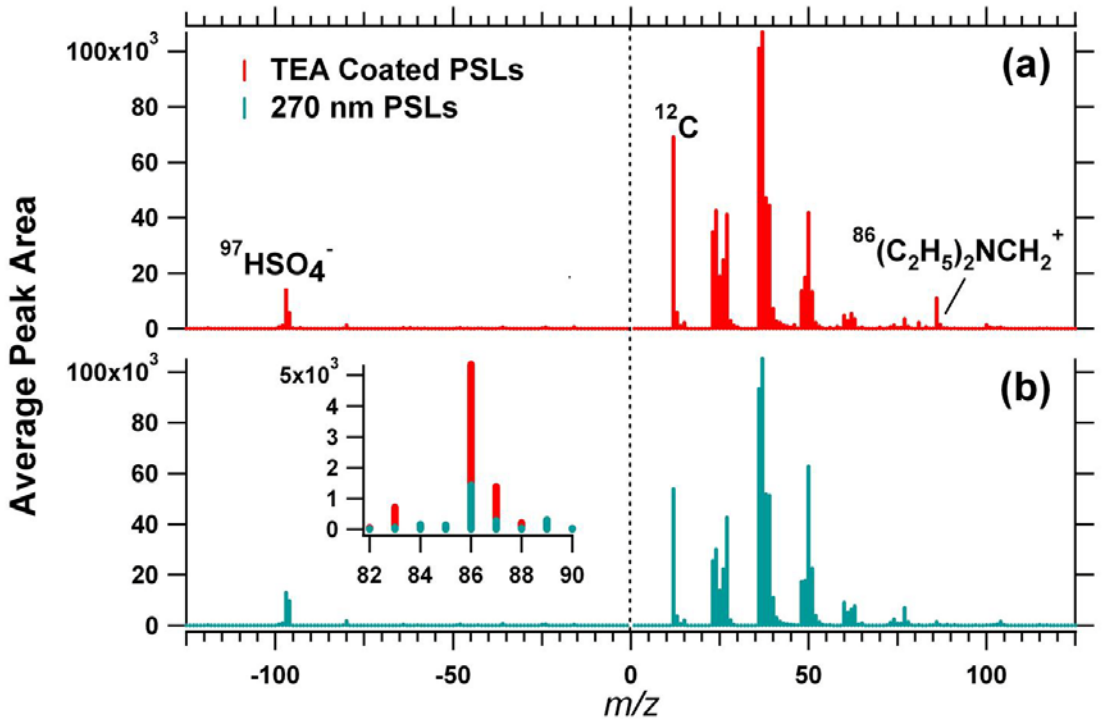

Figure 38: Average mass spectra of (a) PSLs coated with TEA and (b) uncoated 270 nm PSLs. The inset shows a comparison of the *m/z* 86 peak intensities.

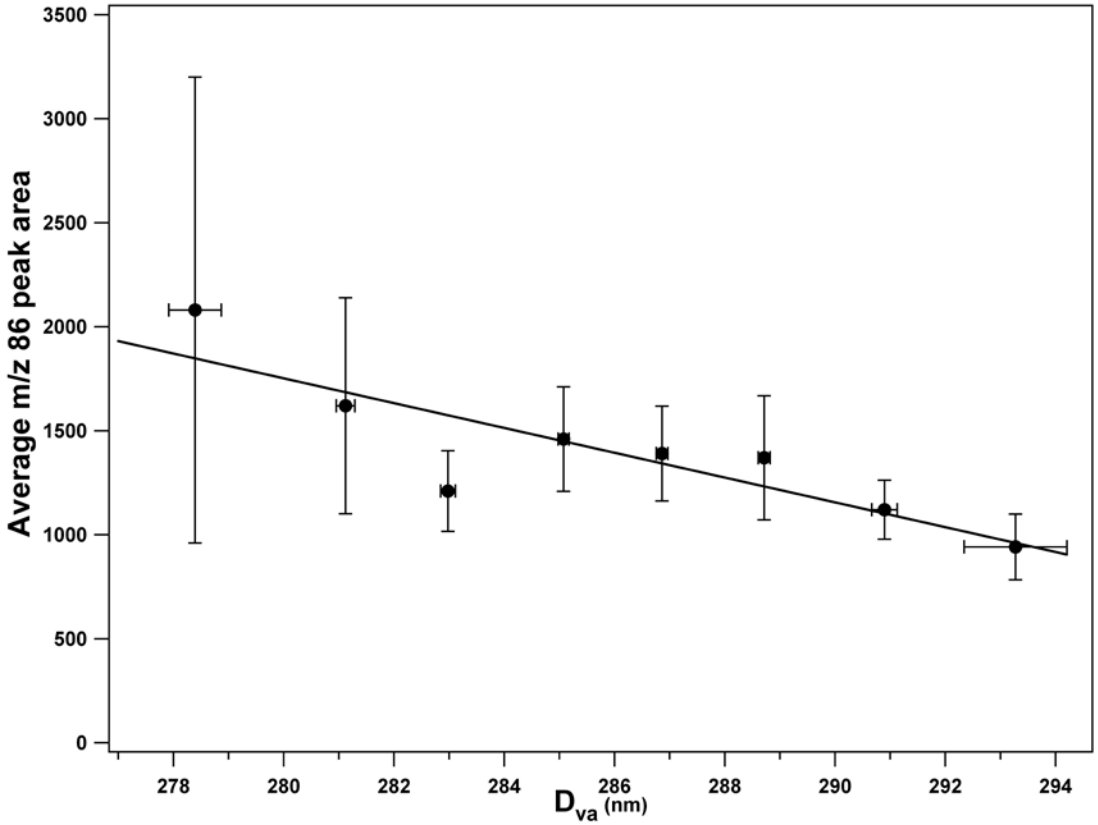

Figure 39: Absolute area of *m/z* 86 vs vacuum aerodynamic diameter for the TEA-coated PSLs.

TEA coated PSLs displayed a shift to larger mobility diameter D_m, consistent with an increase in particle volume upon coating. These observations and the following relationship between D_{va} and D_m (34):

$$\rho_p = \frac{D_{va}}{D_m}\rho_0 \qquad (3)$$

where ρ_p is the particle density and ρ_0 is the standard density (1 g/cm^3), indicate a decrease in particle density upon addition of TEA, consistent with the relative material densities of PSLs (1.05 g/cm^3) and TEA (0.75 g/cm^3). The particle density of TEA coated aerosols is therefore given by:

$$\rho_p = \frac{\rho_{PSL}V_{PSL} + \rho_{TEA}V_{TEA}}{V_p} \qquad (4)$$

where V_p is the coated particle volume, which can be obtained from D_m, as this measurement is not influenced by particle density and the partitioning of TEA is not expected to alter the particle morphology of the spherical seed PSLs. Rearranging Equation 4 and substituting for ρ_p ultimately yields:

$$m_{TEA} = \rho_{TEA}V_{TEA} = \pi/6\,(D_m^2 \cdot D_{va} \cdot \rho_0 - D_{PSL}^3 \cdot \rho_{PSL}) \qquad (5)$$

where m_{TEA} is the mass of TEA. The D_m values corresponding to each D_{va} bin were estimated by:

$$D_{m,equiv} = D_{va} - (\overline{D_{va}} - \overline{D_m}) - 2(D_{va} - \overline{D_{va}}) \qquad (6)$$

where D_{va} represents the average vacuum aerodynamic diameter of a given size bin and $\overline{D_{va}}$ and $\overline{D_m}$ represent the mode diameters of the full ATOFMS and SMPS size distributions, respectively. The wide size bins (~10 nm) used in the SMPS scans precluded direct correlation to the 2nm D_{va} used in the ATOFMS data. Substituting these estimated D_m values into Equation 5 yields the average mass of TEA on individual particles within each size bin.

The corresponding peak area of the *m/z* 86 amine marker was then related to the calculated amine mass to generate a calibration curve (**Figure 40**). To account for detector sensitivity and voltage setting changes between 2005 and 2009, the total summed peak areas of the average mass spectra of uncoated 270 nm PSLs run on the A-ATOFMS during SOAR and this amine calibration experiment were compared, and the peak areas in this experiment were scaled to accommodate for any changes in overall mass spectral intensities. Finally, the calibration experiment data was fit using a linear regression forced through the origin and weighted by the standard deviation in *m/z* 86 peak area. The amine mass present in the aged OC particles in SOAR-1 and SOAR-2 was determined by inserting the average peak areas at each temperature into the calibration curve. All reported uncertainties represent the 95% confidence intervals. The errors associated with the derived ambient amine masses are primarily due to uncertainties in the amine calibration experiment; in general, the 95% confidence intervals associated with the average ambient *m/z* 86 peak area was less than ~6% of the value, with the exception of the low SOAR-2 areas at 201-230 ºC, where errors of 13-17% were observed.

The mass fraction of TEA was also calculated by ratioing the calculated TEA mass to the total particle mass, estimated from mean particle volume at each temperature

(calculated from the mean particle vacuum aerodynamic diameter) and the aged OC particle effective density determined during SOAR-2 (1.38 ± 0.06 g/cm^3)

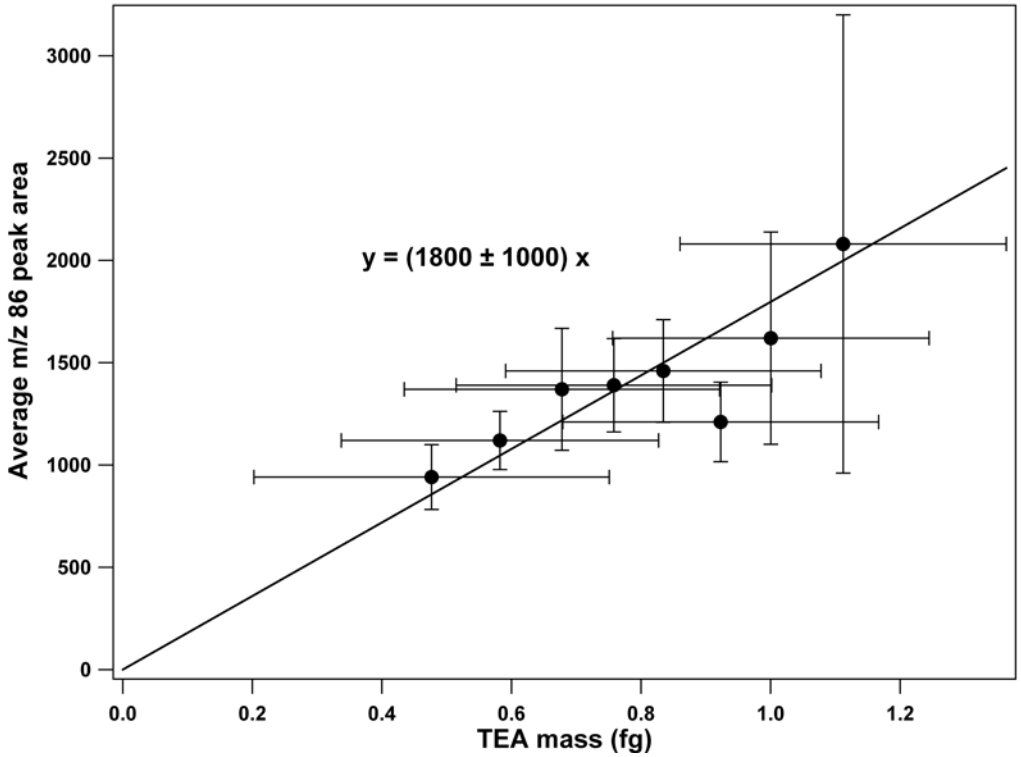

Figure 40: Absolute area of *m/z* 86 vs derived TEA mass for the TEA-coated PSLs.

(194). The mass fraction of amines present as aminium salts within the SOAR aged OC (nitrate-sulfate) particles was calculated based on the mass of TEA present at 230°C. While a combination of nitrate and sulfate salts were present in the aged OC particles, the masses of aminium salts were calculated for three extremes: 100% H-TEA-NO_3, 100% H-TEA-HSO_4, and 100% $(H\text{-}TEA)_2SO_4$. Given the number of moles of TEA calculated to be present in the 230ºC and the molecular weights of the various aminium salts, the masses of aminium salts were estimated and compared to the calculated total particle masses of the unheated and 230°C heated particles. In this way, the mass fractions were estimated for a range of possible aminium salt species. To reduce error, average fractions of amines remaining at each temperature are based on *m/z* 86 absolute peak areas, a reasonable assumption considering the observed proportionality of *m/z* 86 peak area to mass.

iii. Results and Discussion

Particles containing internally mixed organic carbon, ammonium, nitrate, and sulfate, herein referred to as the aged OC particle type, comprised ~60% by number of all particles across the entire size range from d_{va} ~150-1000 nm during SOAR-1 (summer) and SOAR-2 (fall) (see **Figure 35**). As shown in **Figure 41**, the unheated aged OC particle type was characterized by carbonaceous marker ions at *m/z* 12(C^+), 27($C_2H_3^+$/CHN^+), 36(C_3^+), 37(C_3H^+), and 43(CH_3CO^+/$CHNO^+$) (195), as well as ammonium (*m/z* 18, NH_4^+), nitrate (*m/z* -62, NO_3^-, and -125, $H(NO_3)_2^-$), and sulfate (*m/z*

-97, HSO_4^-), all indicators of the aged nature of the Riverside aerosol (158). These particles were also characterized by marker ions for

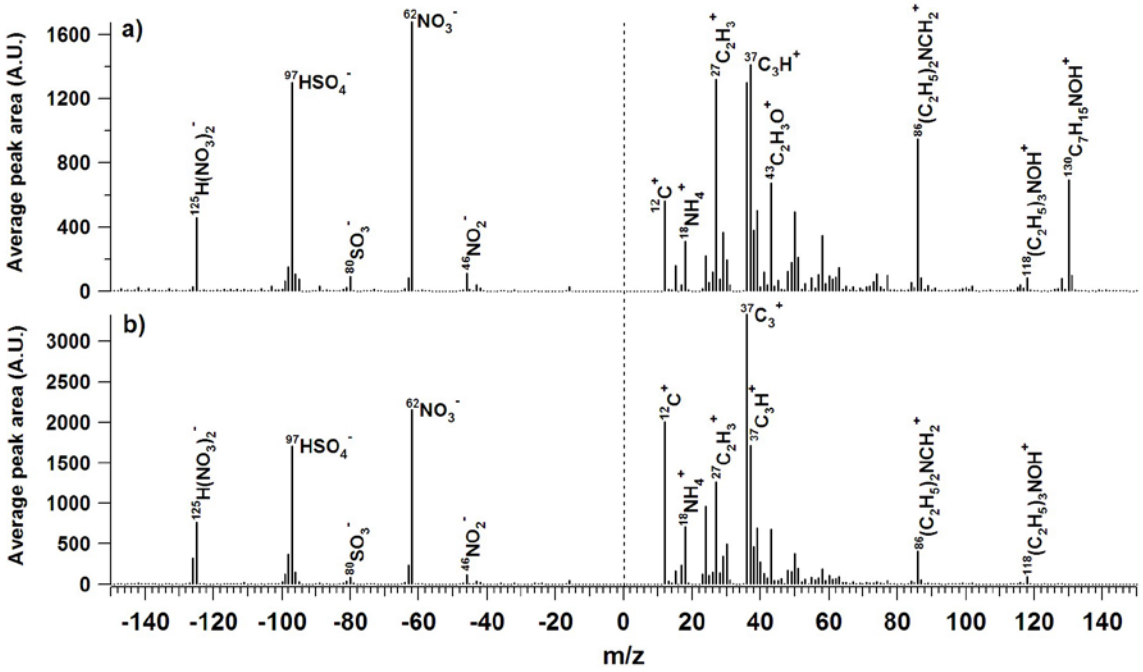

Figure 41: Average positive and negative mass spectra of the unheated aged OC (nitrate-sulfate) particles during (a) summer and (b) fall. Peak areas are reported in arbitrary units (A.U.).

alkylamines, *m/z* 86($(C_2H_5)_2NCH_2^+$) and 102($(C_2H_5)_3NH^+$), as well as oxidized amines, represented by *m/z* 118($(C_2H_5)_3NOH^+$) (39). Previously, Angelino et al. (39) found contributions of triethylamine and diethylamine to these marker ions; herein, *m/z* 86 is used as a general marker ion for the presence of amines. During SOAR-1, SOA was found to comprise ~45-90% of the total submicrometer organic mass depending on time of day (peak morning traffic vs. afternoon photochemical episodes) (196); previous studies have shown lower SOA contributions in the fall due to lower photochemical activity (54). In addition, oligomers (at *m/z* -200 to -400) were observed in approximately half of the unheated aged OC particles in both the summer and fall, although higher mass nonvolatile oligomers were detected in the summer (197).

In the summer, the presence of an intense peak at *m/z* 130, not observed in the fall, is proposed to be either an oxidized form of triethylamine or the $[MH]^+$ peak of N,N-diethylpropionamide ($C_7H_{15}NO$), which may be formed through the following dehydration reaction between propionic acid and diethylamine, observed as a small peak at *m/z* 58 $[MH]^+$ (39).

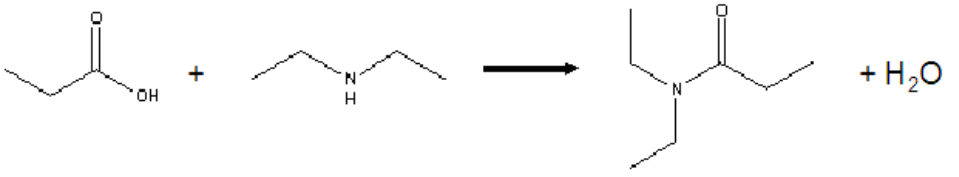

(7)

Propionic acid, the third most abundant gas phase organic acid in the LA basin, is formed primarily through secondary photochemical reactions and reaches its highest concentrations during summer smog episodes in the eastern LA basin (198,199).

Particle phase amide formation has been suggested to be significant in the polluted, ozone-rich troposphere (183). With a calculated vapor pressure of 0.444 Torr at 25°C, N,N-diethylpropionamide is significantly less volatile than it's parent compound diethylamine with a calculated vapor pressure of 218 Torr (25°C) (Advanced Chemistry Development, 200); likewise, *m/z* 130 does not vaporize from the particle phase with heating to 230°C. The peak at *m/z* 130 has been also been observed in chamber experiments conducted during July 2006, probing the gas-to-particle partitioning of TEA via homogeneous reaction with nitric acid (**Figure 42**), similar to the experiment completed by Angelino et al. (39). The experimental setup was similar to that described above for the amine coating experiments with the following key differences: (1) the atomizer and diffusion dryers were not used as a seed aerosol was not provided; (2) the flow rate of filtered ambient air into the chamber was 4.0 $L \cdot min^{-1}$, providing shorter residence time; (3) the chamber contained two flasks containing nitric acid and TEA. In previous chamber experiments by Angelino et al. (39), amine oxidation products were also observed due to gas-phase oxidants present in the filtered air utilized.

To probe the specific associations between amines, ammonium, nitrate, and sulfate within the SOAR aged OC particles, ternary plots of the relative distributions of the peak areas of ammonium (*m/z* 18), amines represented by *m/z* 86, nitrate (*m/z* -62), and sulfate (*m/z* -97) at different temperatures for individual aged OC particles are shown in **Figure 43**. The relative amounts and associations of either nitrate (a,c) or sulfate (b,d) with amines and ammonium are displayed for both seasons. A particle containing primarily amines relative to ammonium, nitrate, and sulfate would appear at the top vertex, primarily ammonium at the right vertex, and nitrate or sulfate would appear at the

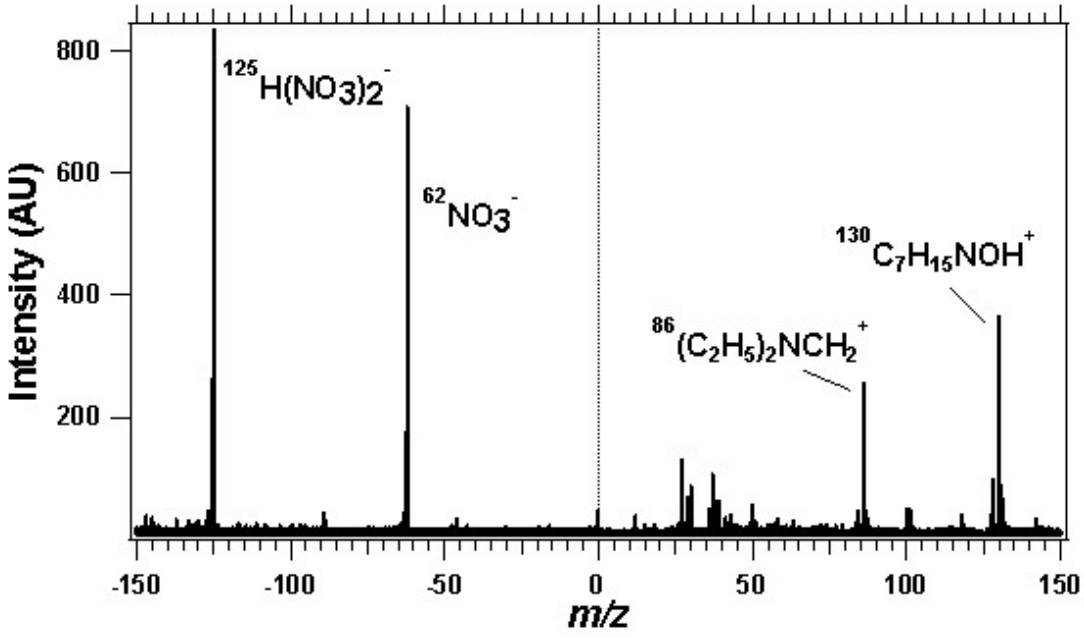

Figure 42: Positive and negative mass spectra of a single particle exhibiting *m/z* 130 measured during TEA-nitric acid chamber experiments.

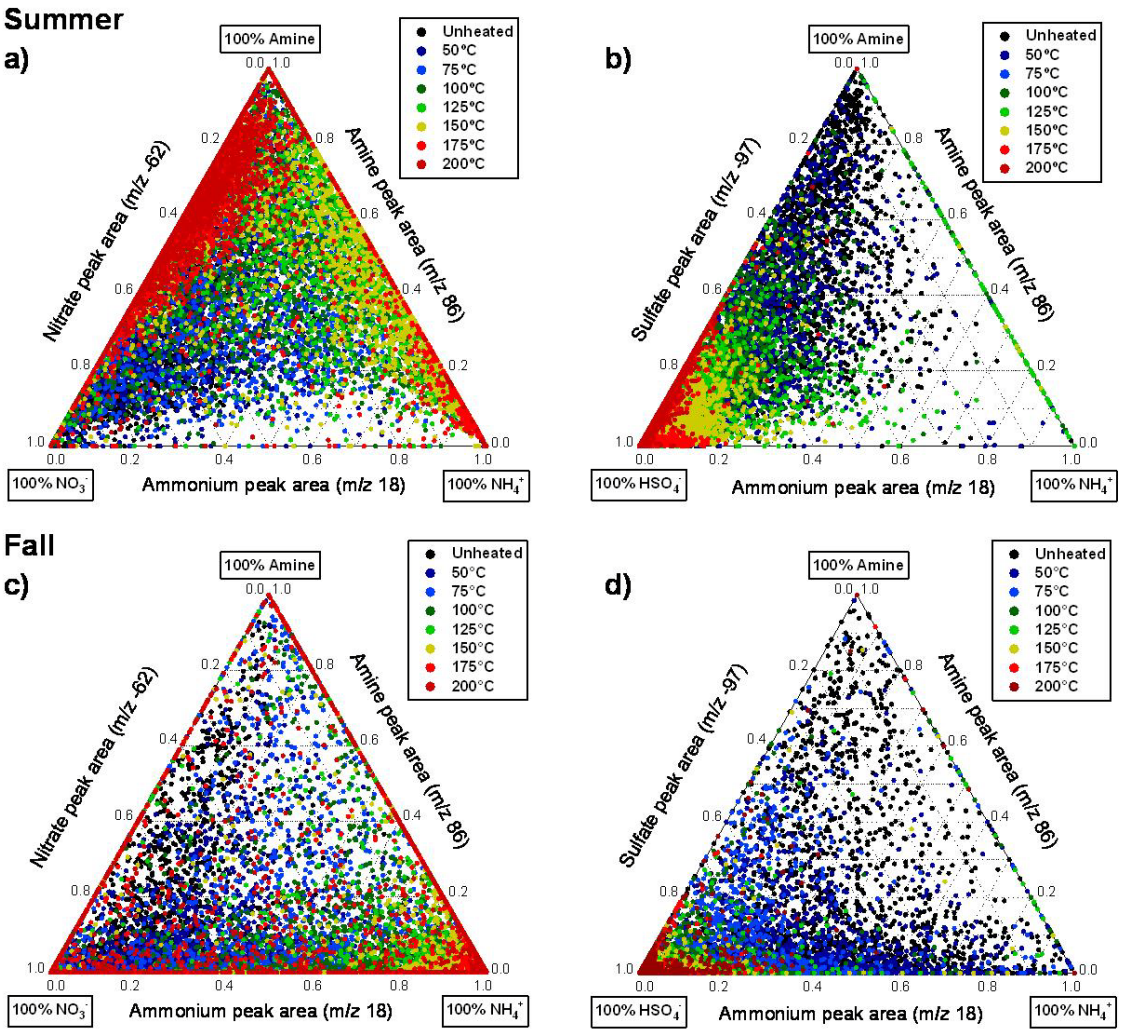

Figure 43: Summer (a,b) and fall (c,d) ternary plots show the relative distributions of peak areas of ammonium (*m/z* 18 (NH_4^+)), amines (*m/z* 86 ($((C_2H_5)_2NCH_2^+)$), nitrate (*m/z* -62 (NO_3^-)), and sulfate (*m/z* -97 (HSO_4^-)) for the unheated and heated (54-230°C) aged OC (nitrate-sulfate) particles. Random samples of ~2,000 single particles are plotted for each temperature.

left vertex. In the summer, the particles are distributed along the amine-nitrate and amine-sulfate axes, suggesting nitrate and sulfate are more strongly associated with amines compared to ammonium. This strong correlation between amines and nitrate and sulfate at 230 °C in the summer supports the presence of aminium nitrate and sulfate salts which are non-volatile, as predicted by Pankow (185). However, in the fall, the unheated particles are distributed primarily along the ammonium-nitrate and ammonium-sulfate axes, suggesting nitrate and sulfate are more strongly associated with ammonium compared to amines. The lack of aminium salts in the fall is because the particles were neutralized and hence the unbound amines were readily volatilized at temperatures below 113 °C, as discussed below. Ammonium and nitrate volatilized at temperatures less than 113 °C, consistent with previously reported volatilization temperature (~48-89 °C) (201). Thus, in the summer, aminium nitrate and aminium sulfate remained in the particles at 230 °C, compared to primarily ammonium sulfate in the fall.

To calculate the relative fraction of amines remaining at each TD temperature, the average absolute peak area of *m/z* 86($(C_2H_5)_2NCH_2^+$) at each temperature was divided by that observed for the unheated aged OC particles (**Figure 44a**). Next, to quantitatively assess the contribution of amines to particle mass, the average amine mass in the aged OC particle type (**Figure 44b**) was determined using a triethylamine mass/peak area calibration curve derived from the amine mass calibration experiment. Using the average vacuum aerodynamic diameter measured for the aged OC particle type at each TD temperature, the average mass fraction of amines per particle was calculated (**Figure 44**). For the SOAR unheated aged OC particles, approximately twice as much amine mass was present in the summer (0.5 ± 0.3 fg/particle; 1.7 ± 0.9%) compared to the fall

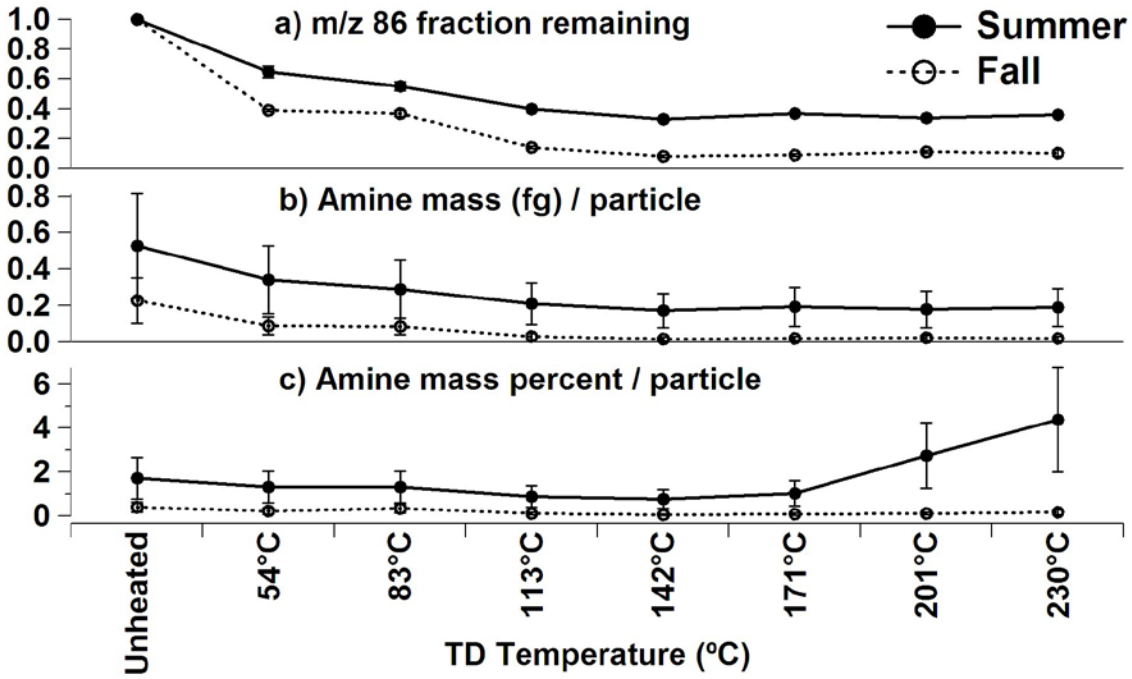

Figure 44: For aged OC (nitrate-sulfate) particles, the (a) fraction of *m/z* 86 peak area remaining over the range of thermodenuder temperatures from 54-230 °C is shown relative to the unheated particles (ambient temperature averages of 22.9 °C and 15.6 °C in the summer and fall, respectively). In addition, the (b) amine mass/particle and (c) amine mass percent/particle are shown for each temperature.

(0.2 ± 0.1 fg/particle; 0.4 ± 0.2%). During both the summer and fall, the amine mass/particle decreased with increasing temperature to 113 °C and then stabilized at ~0.2 ± 0.1 fg/particle and less than 0.1 fg/particle, respectively. These results are consistent with the vaporization of neutral diethylamine and triethylamine up to ~113 °C (boiling points of 57.3 ± 8.0 °C and 90.5 ± 8.0 °C, respectively (Advanced Chemistry Development, 202)). The amines remaining above 113 °C must be in the form of aminium salts. Consistent with the association of amines with nitrate and sulfate in the summer, 36 ± 1% of the amines present at ambient temperature remained in the aged OC particle type at 230 °C in the summer. However, in the fall, only 10 ± 2% of the amines remained at 230 °C, consistent with the decreased abundance of aminium salts due to high levels of ammonium in the particles, as discussed below. Similarly, in the summer,

a greater fraction (13 ± 1%) of nitrate remained at 230 °C compared to the fall (4 ± 1%) (**Figure 45**), consistent with more aminium nitrate salts present in the summer compared to the fall. However, as shown in **Figure 43**, a higher fraction of aminium salts was in the form of aminium sulfate, compared to aminium nitrate; this is likely due to the fact that sulfuric acid is a stronger acid than nitric acid (pKa -3.19 ± 0.15 vs. -1.4, respectively) (Advanced Chemistry Development, 202). At 230 °C, amines represented 4 ± 2% by mass/particle in the summer, compared to only 0.2 ± 0.1% by mass/particle in the fall. The increasing amine mass fraction above 171 °C in the summer was due to the volatilization of other species leaving behind primarily aminium salts and ammonium sulfate; whereas, in the fall, the amine mass fraction did not increase with temperature due to the minor contribution of aminium salts. Considering the potential nitrate, bisulfate, and sulfate salts of triethylamine, the aminium salt mass fraction at 230 °C in

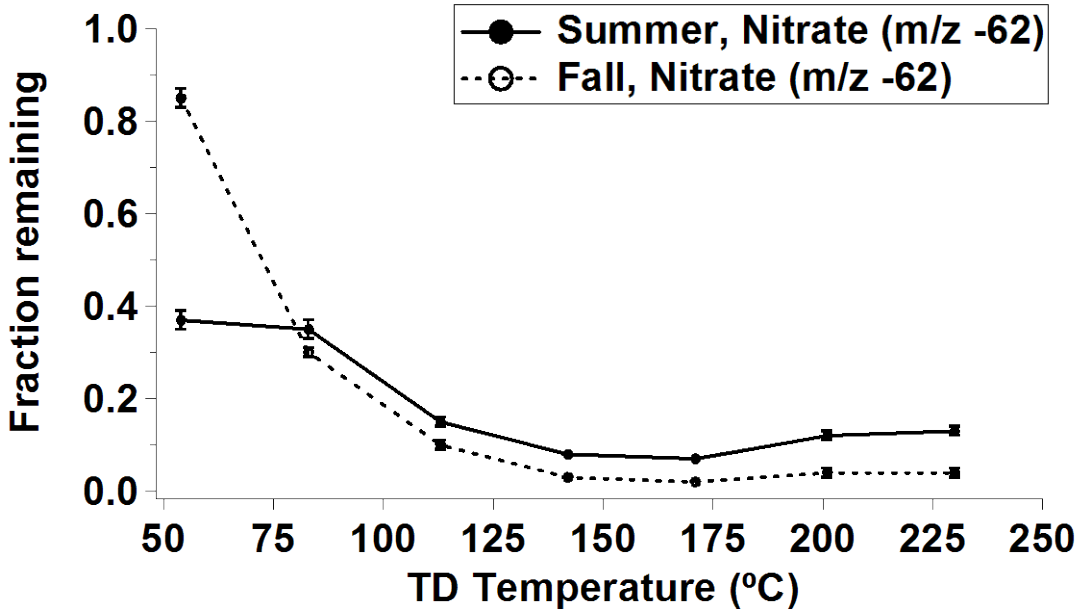

Figure 45: Relative fractions of nitrate (*m/z* -62 (NO_3^-)) remaining on the aged OC (nitrate-sulfate) particles at each TD temperature during SOAR-1 and SOAR-2.

the aged OC (nitrate-sulfate) particles was estimated at ~6-9% in the summer compared to less than 1% in the fall. In the unheated particles, aminium nitrate and sulfate salts were found to contribute ~1% and ~0.6% to the total particle mass in the summer.

Although not the focus of this Chapter, an amine-dominant particle type, comprised ~5-8% by number of the particles ~200-700 nm in diameter during both SOAR-1 and SOAR-2. The mass spectra were dominated by *m/z* 86($(C_2H_5)_2NCH_2^+$) with less intense amine marker ions at *m/z* 58($C_2H_5NHCH_2^+$), 102($(C_2H_5)_3NH^+$), and 118($(C_2H_5)_3NOH^+$) (39); nitrate and sulfate were observed in the negative ions. Using the calibration curve derived herein, these unheated particles were found to be 18 ± 10% and 12 ± 6% amine by mass fraction during the summer and fall, respectively. However, as discussed in Chapter 4, the amine-dominant particle type nearly disappears at ~113 °C, consistent with the volatilization of neutral amines and the reclassification of the particles within the aged OC type. This is shown by the amine mass/particle decreasing from 7 ± 4 fg/particle at ambient temperature to 4 ± 3 fg/particle at 113 °C in these amine-dominant particles in the summer; likewise, in the fall, the amine-dominant particles

contain 6 ± 3 fg amines/particle at ambient temperature and 2 ± 1 fg amines/particle at 113 °C.

Several possible explanations exist for higher amine mass concentrations in the unheated aged OC particle type in the summer compared to the fall. Ammonia has a higher vapor pressure (5990 Torr at 25 °C) than triethylamine and diethylamine (56.1 and 218 Torr at 25 °C, respectively) (Advanced Chemistry Development, 202). During the summer, higher ambient temperatures were observed (17.6-30.9 °C with a mean of 22.9 °C) compared to the fall (8.4-26.1 °C with a mean of 15.6 °C). While ammonia and amines are emitted from the same sources (178,179), primarily the Chino dairy area to the west of Riverside, their differing vapor pressures impact initial volatilization at the source during the different seasons, likely causing more ammonia and amines to be present in the vapor phase in the summer (203); however, gas-phase concentrations of these species during SOAR were not measured. The lower vapor pressure of the amines compared to ammonia allowed them to more readily partition to the particle phase in the summer at the higher ambient temperatures observed; however, the particle-phase chemistry impacted the protonation and gas/particle partitioning of the amines once in the particle phase. At the lower fall ambient temperatures, ammonia competes with amines to form ammonium nitrate and ammonium sulfate/bisulfate (187) which is supported by the greater particle phase ammonium concentrations (2.30 ± 0.04 times) observed in the aged OC particle type in the fall compared to the summer. This observation is consistent with previous studies showing higher concentrations of ammonium nitrate in the eastern LA basin in the fall (up to ~50% of the fine aerosol mass) (150,204). Thermodynamic calculations have shown that increasing ammonia/amine gas-phase ratios from 100 ppt/10 ppt to 1000 ppt/1 ppt led to lower predicted fractions of protonated amines in aqueous nanometer-sized particles (60.5% vs. 1.5%) (187). In addition to gas-phase concentrations, Henry's Law constants (K_H) and acid dissociation constants (pK_a) must be considered in the prediction of the partitioning of amines relative to ammonia (187). Triethylamine is a stronger base than ammonia (pK_a 10.62 ± 0.25 vs. 9.24 ± 0.10) (Advanced Chemistry Development, 202) and has a Henry's Law constant of similar magnitude (K_H 29 M atm^{-1} vs 62 M atm^{-1}) (187), allowing the amines to compete for protons even when at lower concentrations.

In acidic particles, amines will become protonated and remain in the particle phase, forming aminium salts (185,187); thus one expects to see seasonal differences in the partitioning of amines due to changes in particle acidity. In the summer, the aged OC particles were more acidic, as shown by a more intense (1.39 ± 0.04 times) sulfuric acid cluster ion peak at *m/z* -195 ($H_2SO_4HSO_4^-$), a proxy of non-neutralized sulfate and particle acidity. In addition, higher oxalate (*m/z* -89($COOHCOO^-$)) ion peak areas (1.62 ± 0.03 times) were observed in the summer compared to the fall, suggesting that, in addition to nitric and sulfuric acid, organic acids could also form aminium salts, as suggested by Smith et al. (186) and Barsanti et al. (187). While oxalic acid, for example, has a higher pK_a than nitric acid (1.38 ± 0.54 vs -1.4) (Advanced Chemistry Development, 202), it has a substantially lower vapor pressure (2.51 x 10^{-6} Torr vs 49.8 Torr) (Advanced Chemistry Development, 202), allowing it to partition more readily to the particle phase to form aminium organic salts. Due to the increased particle acidity in the summer, a higher amine fraction is believed to be protonated, leading to increased concentrations of aminium salts in the summer compared to the fall, as observed.

Further, we hypothesize that the higher atmospheric water content in the summer (15.9-20.5 mMol/Mol with a mean of 18.9 mMol/Mol) compared to the fall (5.5-16.5 mMol/Mol with a mean of 12.6 mMol/Mol) caused more aminium salts to dissolve within the particle phase, causing an equilibrium shift of the amines from the gas to the particle phase (39). This equilibrium shift would further explain the higher amine mass concentrations in the unheated aged OC particles in the summer compared to the fall. In this way, aminium salts may contribute to aerosol growth, as suggested by Barsanti et al. (187).

Generally, pH is estimated using an ion balance of ammonium with nitrate and sulfate. However, previous studies have shown differences in calculated and measured pH for submicrometer aerosols (205). Based on the relatively significant contribution of amines shown during this study, it is recommended that particle acidity calculations take into account the presence of amines which act as even stronger bases than ammonia in atmospheric aerosols. Thus, for the aged OC (nitrate-sulfate) particles in this study, the particles would be predicted to be more acidic than in actuality based on only ammonium, sulfate, and nitrate concentrations. To illustrate this point, relative acidity ratios are calculated for the SOAR-1 and SOAR-2 aged OC particles; defined as the sum of the absolute average peak areas of nitrate (*m/z* -62 (NO_3^-)) and sulfate (*m/z* -97(HSO_4^-)) divided by ammonium (*m/z* 18(NH_4^+)) (i.e., the typical ion balance method used for calculating pH) or the sum of ammonium and amines (*m/z* 86($(C_2H_5)_2N{=}CH_2^+$)). These resulting ratios are shown in **Figure 46**. In the summer, the relative acidity ratio is overpredicted by a factor of 4 when amines are not taken into consideration, showing the significant role of amines as bases in the summer. In the fall, the addition of amines to the relative acidity ratio does not change the value dramatically (factor of 1.6) when ammonium is the dominant base.

These measurements represent the first quantification of the volatility behavior and mass contribution of amines to individual aged atmospheric particles. During SOAR, the partitioning of amines between the gas and particle phases depended strongly on particle acidity. The more acidic particles in the summer resulted in protonation of the

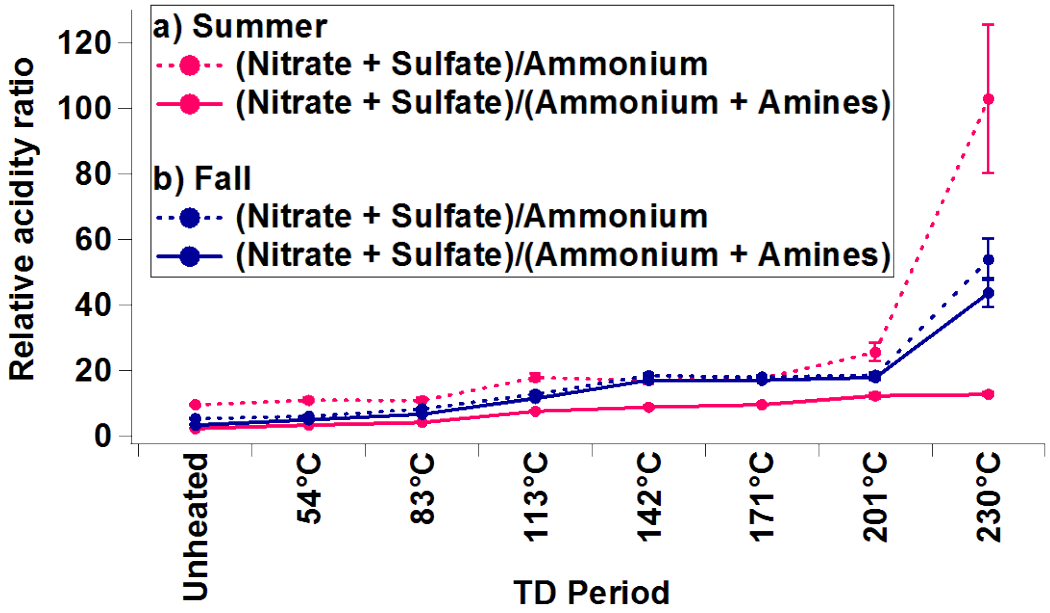

Figure 46: Relative acidity ratios for summer and fall for each thermodenuder period (unheated, 54°C, 83°C, 113°C, 142°C, 171°C, 201°C, 230°C) for the aged OC (nitrate-sulfate) particles. The ratios are defined as the sum of the absolute average peak areas of nitrate (*m/z* -62 (NO_3^-)) and sulfate (*m/z* -97 (HSO_4^-)) divided by ammonium (*m/z* 18 (NH_4^+)) or the sum of ammonium and amines (*m/z* 86 ($(C_2H_5)_2NCH_2^+$)).

amines, causing the formation of aminium sulfate and nitrate salts, which did not volatilize at temperatures up to 230 °C. These amine salts represent low-volatility organic carbon species that could potentially be missed by thermal analysis methods. In the fall, higher particulate ammonium concentrations and more basic particle cores produced fewer aminium salts, causing 86 ± 1% of the amines to volatilize below 113 °C. The abundance of organic carbon mixed with amine salts, as observed in this study, may form a barrier that prevents the salts from remaining at equilibrium with the gas phase (176). Previous chamber studies have found aminium nitrate salts repartition back to the gas phase under low RH conditions (<10%) (176); however, under the conditions of this study, this revolatilization process did not occur because the presence of water caused the aminium salts to dissolve, shifting the equilibrium of the gas-phase amines toward the particle phase. Further, previous chamber studies have not examined the partitioning of the amine salts with respect to pH, shown in this SOAR data to be a critical parameter affecting gas/particle partitioning. Laboratory studies of the competition between ammonia and different amine species for sulfuric, nitric, and organic acids, as a function of temperature, RH, and particle size, and the relative abundance of amines and ammonia are planned to further understand the partitioning of amines in the atmosphere. Further, it is important to note that the average bulk pH of a collection of ambient particles may in fact not be representative of the pH of any individual particle; thus, the single-particle mixing state of atmospheric aerosols must be used as a measure of pH to fully understand the partitioning of semivolatile species such as amines in gas/particle partitioning processes.

iv. Acknowledgements

This work was supported by the National Science Foundation (NSF ATM-0321362) and the California Air Resources Board (CARB 04-336). Together Lindsay Hatch, supported by an NSF graduate research fellowship, and I completed the amine mass calibration; Lindsay wrote the amine mass calibration method portion of this Chapter and contributed to discussions of the data. Prof. Paul Ziemann (UC-Riverside), Ken Docherty (CU-Boulder), the UC Riverside Air Pollution Research Center, and the Prather Group, particularly Gary Poon, Xueying Qin, Laura Shields, and Stephen Toner, provided support during SOAR. Alex Huffman (CU Boulder) and Prof. Jose Jimenez provided and ran the TD system, developed under EPA sponsorship (STAR R831080). Megan McKay and the Goldstein group (UC-Berkeley) provided the atmospheric water content and ambient temperature data. The California Air Resources Board provided $PM_{2.5}$ mass concentrations for the Rubidoux site.

6. Inter-annual Comparison of Ambient, Single-Particle Chemical Mixing State in Riverside, CA

i. Introduction

Atmospheric particles are known to cause severe adverse health effects (96). For instance, fine particulate matter ($PM_{2.5}$, particles with aerodynamic diameters $\leq$2.5 μm) has been linked to increases in cardiovascular and pulmonary diseases, leading to elevated mortality and morbidity (110). Epidemiological studies have applied generalized additive models to time series data to estimate associations between exposure to $PM_{2.5}$ and the diseases mentioned above (206). Improvement of these models based on temporal changes in $PM_{2.5}$ is important for pollution regulation, which can minimize the health effects of these particulates. Urban aerosols specifically contribute to these health effects and are of interest because 1) they represent a significant fraction of $PM_{2.5}$ mass concentrations (148) and 2) better approximations based on measurements are needed to improve the representation of urban aerosols in models and pollution regulations (207).

The Los Angeles (LA) Basin is recognized for some of the highest levels of urban particulate pollution in the United States, especially the city of Riverside, which is ~50 miles east of downtown LA (208). Westerly winds transport emissions from LA, which stagnate in Riverside due to the surrounding topography and inversion layer, increasing $PM_{2.5}$ concentrations (209,210). During transport from LA, heterogeneous reactions of particles with trace gases and gas-particle partitioning of secondary species, such as nitrate (158), sulfate (211), ammonium (212), amines (213), and oxidized organics (214) contribute greatly to changes in particle size and chemistry during transport (96,215). Particles that accumulate these secondary species may become more toxic (110). For instance, high levels of ingested nitrate can subsequently cause lethargy or coma for infants (216) and mortality rates have been related to airborne concentrations of sulfate (217). Secondary amines and oxidized organics can increase the rate of blot clots (218) and cause respiratory and cardiovascular problems (219), respectively. Overall, these secondary species can constitute a large fraction of $PM_{2.5}$ in urban areas of the Western US, with organics, nitrate, sulfate, and ammonium equaling ~70% of the total $PM_{2.5}$ mass (220). Therefore, the extent of particle aging could impact how harmful the particles are to human health. This highlights the importance of being able to detect these species in particles.

Meteorology has large impacts on particle chemistry, number, and mass concentrations, even for urban locations (215). Therefore, meteorological influences on $PM_{2.5}$ should be taken into account in models in order to better associate particulate matter with adverse health effects. In Riverside, several previous studies have linked meteorology or gas-phase concentrations with observed particle chemistry (154) or monitored seasonal variation of particulate mass concentrations (45,148,204,221,222). Pastor et al. (2003) observed increases in carbon-rich particles during elevated O_3 levels in the afternoons during a 40-day summer study in Riverside. Fine et al. (2004) and Geller et al. (2004) found the highest $PM_{2.5}$ in the summer months; while in contrast, Chow et al. (1994) and Kim et al. (2000) found higher $PM_{2.5}$ in the winter months. These contradictory results indicate that in order to improve model inputs, it cannot be assumed that the ambient particles are the same each year, based off of results from one study.

Hence, these results show the need for long-term monitoring and inter-annual comparison of particle chemistry that contributes to $PM_{2.5}$.

Incorporating gas-phase species and meteorology from multiple studies over time could help explain long-term changes in $PM_{2.5}$ concentrations and particle chemistry. Most previous studies have utilized off-line bulk filter measurements; however, in this study, real-time, single-particle measurements were used. This technique provides more specific information about particle mixing state with a high time-resolution, which can give more detailed insight into the influence of particulate chemistry on $PM_{2.5}$ concentration trends. Chemical composition analysis of individual particles allows the identification of particle sources and an assessment of particle aging. Here, we examined the role of meteorology (temperature, relative humidity, wind speed, and air mass back trajectories) and gas-phase O_3 on changes in $PM_{2.5}$ mass concentrations and measured single-particle chemistry in Riverside for three consecutive summers (2005-2007).

ii. Experimental

Individual ambient aerosol measurements were taken during the summers of 2005-2007 at the University of California, Riverside (UCR). Measurements were made during the Study of Organic Aerosols in Riverside (SOAR-1) campaign from July 29 – August 15, 2005, as well as subsequent studies from August 10 –21, 2006 and August 29 – September 7, 2007. All data are given in Pacific Standard Time (PST), 1 hour behind local time. Gas-phase O_3, $PM_{2.5}$ mass concentrations, and meteorological measurements, including wind speed, relative humidity, and temperature were acquired from the California Air Resources Board (CARB) Riverside-Rubidoux sampling site, located ~9 miles northwest of UCR in 2006-2007. In 2005, $PM_{2.5}$ mass concentrations and O_3 were acquired from CARB, while meteorological data were acquired from the Professor Allen Goldstein group at the UCR site.

The size-resolved chemical composition of individual particles was measured using aerosol time-of-flight mass spectrometry (ATOFMS). More specifically, a converging nozzle-inlet ATOFMS (measuring particles with vacuum aerodynamic diameter (D_{va}) of 0.1-1.0 μm) was operated in 2005 and 2007, and the ground-based prototype of the aircraft ATOFMS (D_{va} of 0.2-2.5 μm) with an aerodynamic lens inlet was utilized in 2006; these measurements are described in detail elsewhere (127,223). The measurements of the two instruments have been shown to agree on particle chemistry when co-located (223). This comparison focuses on the overlap size region of 0.2-1.0 μm. Briefly, particles enter through differentially-pumped stages, accelerating particles to their terminal velocities. The speed is measured for individual particles via two continuous-wave diode lasers (532 nm). Aerodynamic size is determined by calibration with polystyrene latex spheres of known physical diameters. Individual particles are subsequently desorbed and ionized by a pulsed 266-nm Nd:YAG desorption-ionization laser, creating positive and negative ions, which are detected within the dual-polarity time-of-flight mass spectrometer. In 2005 the ATOFMS analyzed 1 076 812 particles, in 2006 the A-ATOFMS analyzed 1 099 868 particles, and in 2007 the ATOFMS analyzed 939 297 particles.

For detailed analysis, single-particle size and mass spectra were imported into YAADA (www.yaada.org), a software toolkit for analysis using Matlab (The Mathworks, Inc.). An adaptive resonance theory-based clustering method (ART-2a) (35) was then

used to classify and group single-particle mass spectra with a vigilance factor of 0.80, learning rate of 0.05, and 20 iterations followed by regrouping with a vigilance factor of 0.85. ART-2a classifies particles into separate clusters depending on the presence and intensity of ion peaks within the individual particles' mass spectra. For the three studies presented, the most populated 50 clusters accounted for >90% of the total ART-2a classified particles and are representative of the overall aerosol composition. Peak identifications within this paper correspond to the most probable ions for a given mass-to-charge (*m/z*) ratio. The peak area of a specific *m/z* is related to the amount of a specified species on each particle (85,224).

iii. Results and Discussion

a. Impact of meteorology on particulate mass concentrations

Table 7 (and **Figure 47** of the Supplementary Material) gives a synopsis of temperature (T), relative humidity (RH), wind speed (WS), $PM_{2.5}$ mass concentrations ($PM_{2.5}$), and gas-phase O_3 concentration measurements from the summers of 2005-2007 in Riverside, CA. It is important to note that certain parameters were correlated or anticorrelated with $PM_{2.5}$ mass concentrations and that $PM_{2.5}$ averages and temporal patterns changed each year. Of the sampling periods within the three years, 2007 was characterized by the highest Ts (average 28 ºC, maximum 45 ºC) and lowest average RH (56%) with the lowest average $PM_{2.5}$ mass concentration (22 $\mu g/m^3$). 2006 was the characterized by the lowest Ts (avg. 23 ºC, max. 34 ºC) and highest average RH (75%) year with the highest average $PM_{2.5}$ mass concentration (32 $\mu g/m^3$). In 2005, the T (avg. 26 ºC, max. 38 ºC), average RH (71%), and average $PM_{2.5}$ concentration (30 $\mu g/m^3$) were between 2006 and 2007. The strong relationship between average $PM_{2.5}$ mass concentration, temperature, and RH suggest that the majority of the species contributing to $PM_{2.5}$ could be semi-volatile by nature (225).

Yr	Data	Avg.	σ	Range	Avg. Daily Maxima (PST)
2007	$PM_{2.5}$	22 μg/m³	7 μg/m³	5-46 μg/m³	Various
2005	$PM_{2.5}$	30 μg/m³	13 μg/m³	4-79 μg/m³	10:00
2006	$PM_{2.5}$	32 μg/m³	14 μg/m³	10-74 μg/m³	9:00
2007	RH	56%	22%	25-100%	6:00
2005	RH	71%	20%	36-100%	4:00
2006	RH	75%	22%	25-100%	5:00
2006	T	23 °C	10 °C	16-34 °C	13:00
2005	T	26 °C	10 °C	18-38 °C	13:00
2007	T	28 °C	14 °C	16-45 °C	13:00
2007	WS	3.93 m/s	3.09 m/s	0-15 m/s	14:00
2006	WS	4.37 m/s	4.28 m/s	0-25 m/s	15:00
2005	WS	4.40 m/s	2.74 m/s	1-14 m/s	14:00
2006	$[O_3]$	38.8 ppb	29.8 ppb	1-106 ppb	13:00
2007	$[O_3]$	39.5 ppb	33.7 ppb	1-131 ppb	14:00
2005	$[O_3]$	46.4 ppb	39.6 ppb	0-155 ppb	14:00

Table 7: Measurements of $PM_{2.5}$ (μg/m^3), relative humidity (RH, %), temperature (T, °C), wind speed (WS, m/s), and gas-phase O_3 concentrations (ppb) for the sampling periods during 2005-2007. Standard deviations (σ) and measurement ranges are also listed. 'Avg. Daily Maxima' refers to the average time of the daily maximum of each particular factor.

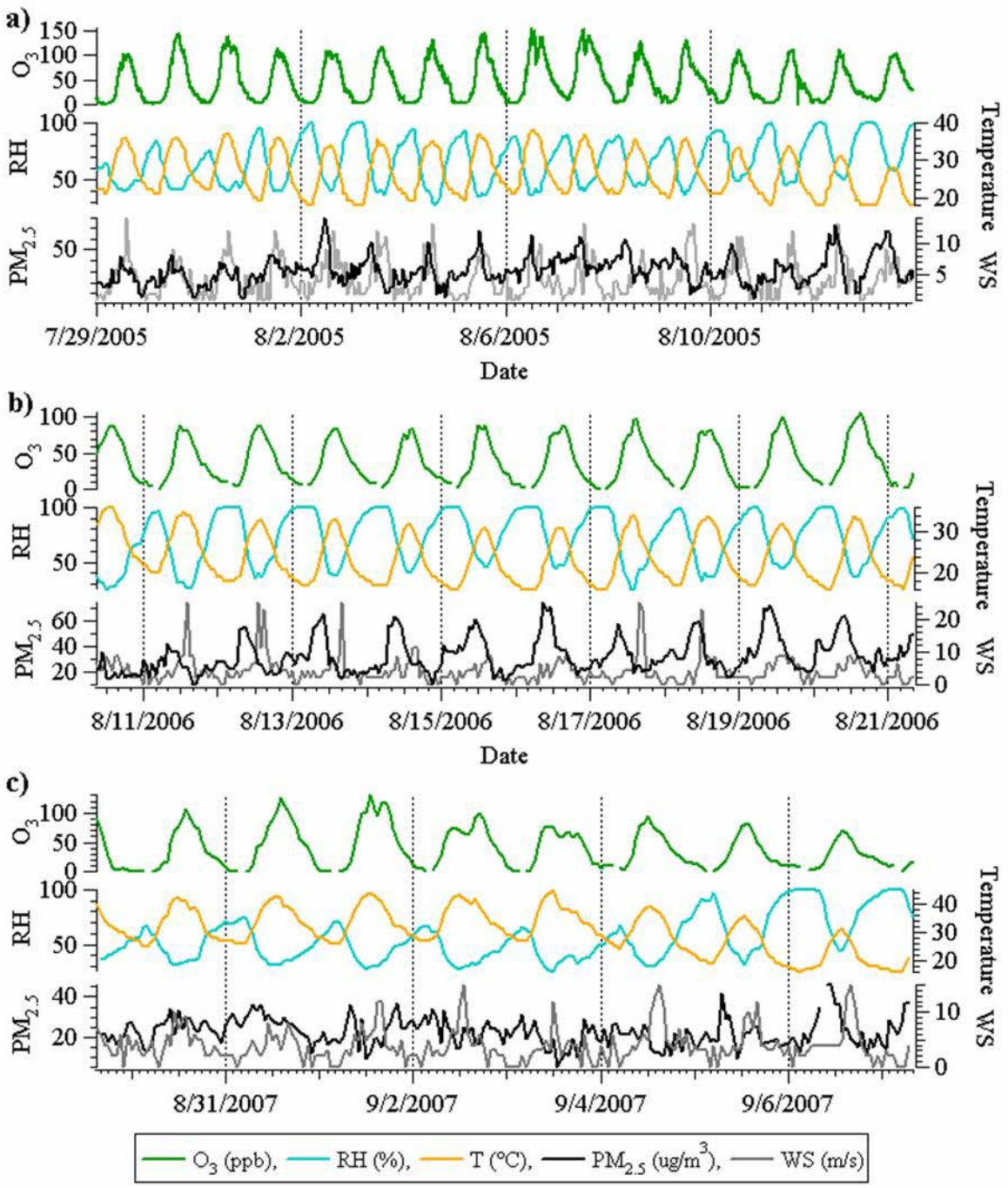

Figure 47: Illustrates the temporal profiles of gas-phase O_3 (ppb, green line), relative humidity (%, blue line), temperature (ºC, orange line), $PM_{2.5}$ mass concentrations (µg/m^3, black line), and wind speed (m/s, grey line) from the three summer studies in Riverside, CA. Plot a) has data from July 29 – August 15, 2005, b) August 10 –21, 2006, and c) August 29 – September 7, 2007. Trends of these measurements are discussed in the main manuscript.

In addition to average $PM_{2.5}$ mass concentrations, $PM_{2.5}$ temporal patterns changed from year-to-year: 2005 had distinctive diurnal variation peaking at 10:00, 2006 was usually diurnal with some days having multiple maxima, and 2007 was variable,

both in number of maxima and peak times, as shown in the Supplementary Information. These differences can be attributed to the meteorology, specifically wind speed (WS). 2005 had very diurnal WS that did not greatly deviate from the average (4.40 m/s, σ = 2.74 m/s), similar to the $PM_{2.5}$ mass concentrations being very diurnal with single daily maxima. The studies in 2006 and especially 2007 had less diurnal $PM_{2.5}$ mass concentrations and sometimes multiple daily maxima due to less uniform temporal profiles of WS. WS influences $PM_{2.5}$ by transporting different numbers of particles with different masses, depending on how consistent and fast the wind is. In addition, air mass trajectories can identify where the particles came from and traveled, and therefore further explain differences in $PM_{2.5}$. **Figure 48** shows the representative air mass back trajectories (AMBTs) calculated using HYSPLIT (226) for the sampling periods from 2005-2007. In 2005, the representative AMBTs originated to the west 80% of the time, while three main northwesterly/southwesterly trajectories were present during 67% of the sampling time in 2006. In contrast, 2007 had highly variable AMBTs due to Santa Ana conditions, which generally have high T, low RH, and high WS originating from a high-pressure system from the northeast (227). Evidence of a Santa Ana in 2007 is confirmed by the easterly inland trajectory from the Mojave Desert area, high average T (43 ºC) and low average RH (69%), leading to low $PM_{2.5}$ concentrations. Santa Ana conditions were not observed in 2005 or 2006, which both had higher $PM_{2.5}$ concentrations than 2007.

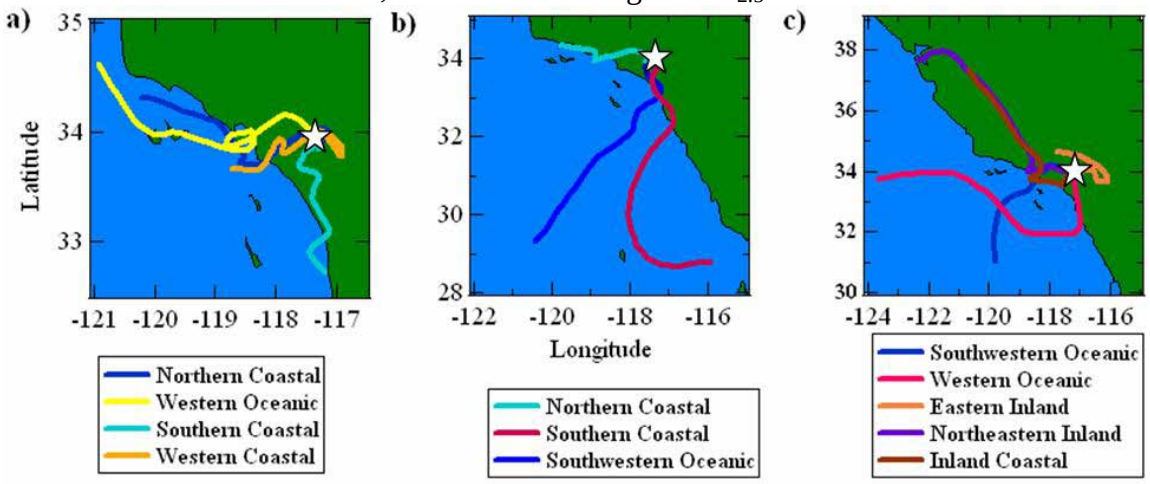

Figure 48: Representative 48-hour HYSPLIT air mass back trajectories in Riverside for a) 2005, b) 2006, and c) 2007. Trajectories are labeled by source wind direction and terrain. The sampling site is represented by the star in each map.

Particle mass is strongly dependent on meteorology and where the particles originate and travel. T and RH can affect mass concentrations by determining what semi-volatile species are in the particle-phase such that high T and low RH permit semi-volatile species to stay in the gas-phase, but low T and high RH lead these species to partition to the particle-phase, adding mass. Winds can also influence particle mass concentrations such that they can control diurnal variations in $PM_{2.5}$. WS and AMBTs affect where the particles come from and how they transform as they are exposed to different conditions in the atmosphere. The mass concentrations of particles are dependent on the source; however, meteorology has a large impact on $PM_{2.5}$ and is different on an inter-annual scale.

b. Overall submicron aerosol chemical composition

Because of year-to-year differences in $PM_{2.5}$, the particles contributing to mass differ chemically and vary by concentration. More detailed analysis of individual-particle chemistry and number fractions can give insight as to what particles are contributing to the $PM_{2.5}$ each year. Further, details on particle mixing states in conjunction with meteorology can help develop more precise parameters for health models and improve pollution regulations. The mass spectral signatures of the ATOFMS particle types presented in this manuscript are similar to those described by Pastor et al. (154) and Qin et al. (208) for previous measurements in Riverside, CA and are described in **Table 8**. The major submicron particle types present during the three summer studies were aged organic carbon (AgedOC), amine-containing, elemental carbon (EC), elemental carbon/organic carbon (ECOC), biomass burning, aged sea salt (AgedSS), and dust; other minor types comprised <10% of the total over the size range of 0.2-1.0 μm.. Representative mass spectra of these particle types are found in the Supplementary Material.

ATOFMS Particle Type	Characterization
AgedOC	Carbonaceous markers at $^{12}C^+$, $^{27}C_2H_3^+$/CHN^+, $^{36}C_3^+$, $^{37}C_3H^+$, $^{43}CH_3CO^+$/$CHNO^+$, and $^{86}(C_2H_5)_2NCH_2^+$
Amine	Contained $^{86}(C_2H_5)_2NCH_2^+$ with less intense amine marker ions at $^{58}C_2H_5NHCH_2^+$, $^{102}(C_2H_5)_3NH^+$, and $^{118}(C_2H_5)_3NOH^+$ and other minor organic carbon peaks
Ammonium	Contained $^{18}NH_4^+$ with less intense organic peaks
EC	Characterized by intense carbon cluster positive and negative ions from $C^{+/-}$ to $C_n^{+/-}$
ECOC	Similar to that of EC with less intense OC and amine ion peaks
Biomass	Contained potassium with less intense carbonaceous positive ions while the negative ions contained nitrate and sulfate
AgedSS	Intense sodium, potassium, nitrate, and sulfate ion markers with smaller ammonium and carbonaceous ion markers
Dust	Inorganic peaks at $^{23}Na^+$, $^{24}Mg^+$, $^{40}Ca^+$, and may contain $^{56}Fe^+$

Table 8: Descriptions of the major ATOFMS particle types from 2005-2007.

c. Assessment of single-particle mixing state and particle aging

It is important to note that the majority of the particles from 2005-2007 were internally mixed or "aged" with secondary species, regardless of particle type: AgedOC, amines, biomass, AgedSS, dust, and ECOC showed evidence of aging based on markers of ammonium ($^{18}NH_4^+$), amines ($^{86}C_5H_{12}N^+$), oxidized OC ($^{43}C_2H_3O^+$/$CHNO^+$), sulfate ($^{97}HSO_4^-$), and nitrate ($^{46}NO_2^-$ and $^{62}NO_3^-$). **Figure 49** illustrates the mixing states of major ATOFMS particle types with secondary species during the 2005-2007 summers. Each square represents the number fraction of each particle type containing a particular *m/z* marker, i.e., the percentage of a particle type aged with a secondary species out of the total number of particles of that type. It is important to note that each particle type may be aged with more than one secondary species. These markers significantly differ each year except for the fraction of particles containing *m/z* 86 within the amine particle type, which will be disregarded as it is a reference spectral marker for this type.

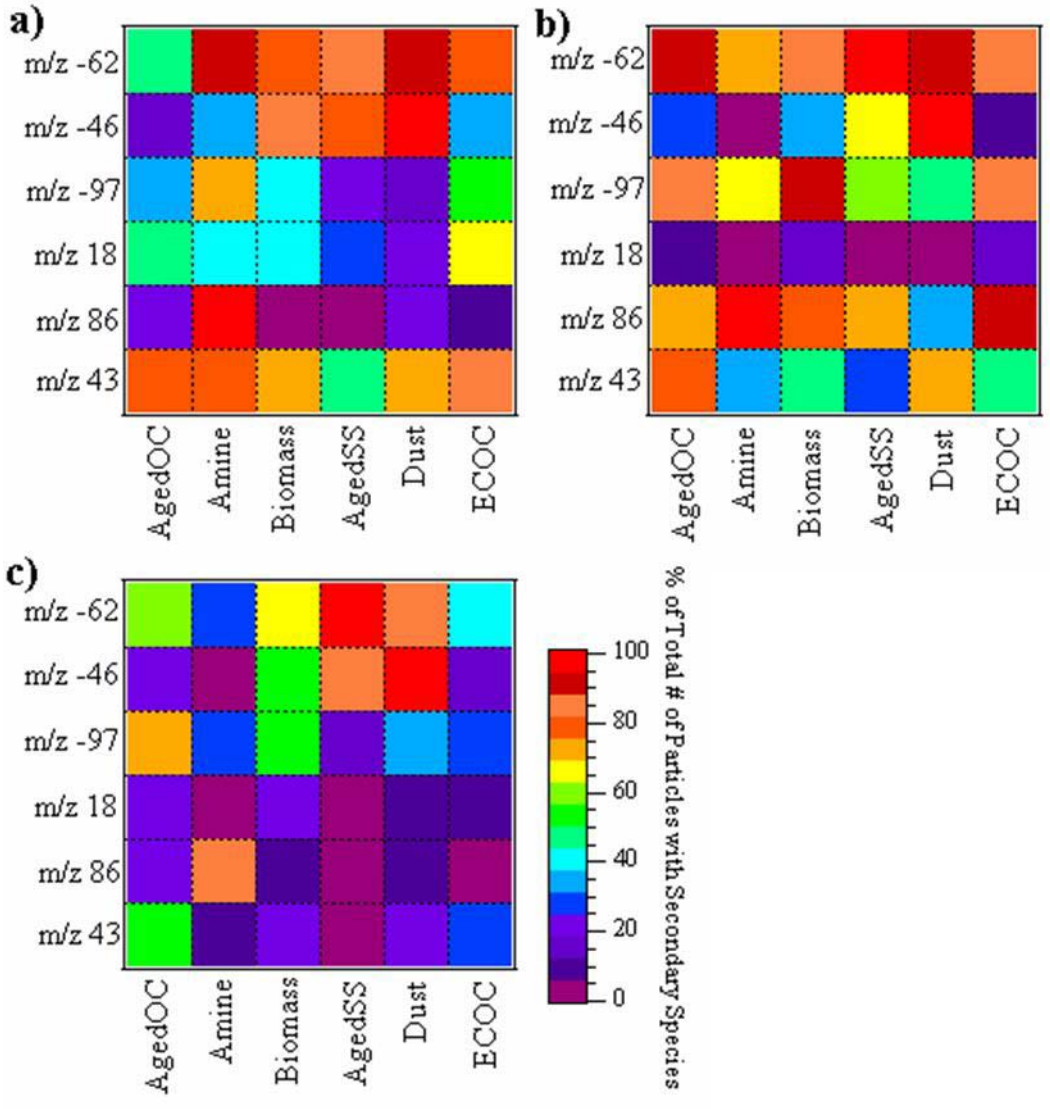

Figure 49: Mixing states of secondary species in major particle types from a) 2005, b) 2006, and c) 2007. The abscissa contains major ATOFMS particle types and the y-axis contains secondary species markers $C_2H_3O^+$ (*m/z* 43), $(C_2H_5)_2NCH_2^+$ (*m/z* 86), NH_4^+ (*m/z* 18), HSO_4^- (*m/z* -97), NO_2^-

(*m/z* -46), and NO_3^- (*m/z* -62). The color scale represents the number fraction of particles within a single particle type that contained each specific marker (secondary species).

Overall, all three years showed the most aging of all particle types with secondary nitrate, ranging from 53-91% of each particle type in 2005, 72-97% in 2006, and 26-95% in 2007. This suggests high nitrate levels were present, which have previously been modeled and observed in Riverside (148,158,228). In addition to nitrate in 2005, the major particle types were aged with oxidized OC (ranging from 48-88% of the total number of each particle type), consistent with the highest O_3 concentrations observed. Because the average O_3 concentration was highest in 2005, this suggests the particles were highly oxidized compared to 2006 or 2007 (particle types aged with oxidized OC = 38-79% and 6-51% of the total number of each particle type, respectively). Aging with sulfate was more apparent in 2006 (particle types aged with sulfate = 51-87% of the total number of each type) than in 2005 specifically on the amine type, which demonstrates acid-base chemistry between $H_2SO_{4(g)}$ and basic amine markers forming aminium sulfates (39,213). Although aminium nitrate salts are more significant in agricultural settings like the surroundings of Riverside, aminium sulfate may form in the presence of high sulfate concentrations (176) and have been previously shown to correlate in Riverside during the summer (213). Also apparent are higher fractions of secondary amines in all particle types (particle types aged with secondary amines = 41-87% of the total number of each type) compared to 2005 and 2007 (particles types aged with secondary amines = 7-27% and 6-24% of the total of each type, respectively). The higher average RH (and lower average T) in 2006 caused semi-volatile species, such as amines, to partition to the particle phase (39). Both 2005 and 2006 had more aging of different organic particle types (AgedOC, amines, ECOC, biomass); however, in 2007 there was more aging of inorganic types such as AgedSS and dust with nitrate (95% and 82% of the total of each type, respectively). This change in mixing state from 2005 and 2006 to 2007 can be attributed to Santa Anas transporting more dust, which readily takes up nitrate (229) and salts from AMBTs originating and traveling over the Pacific Ocean, especially from September 5-7, 2007 as discussed below.

These results show that the relative number of particle types aged with secondary species can change and that aging is not on the same type from year-to-year. The extent of particle aging can be examined by looking at a ratio of a more-oxidized marker (*m/z* 43) to a less-oxidized marker (*m/z* 37) and its relationship to O_3 as shown in the Supplementary Material. Also, these particles largely contribute to $PM_{2.5}$ mass and can change the chemical composition of the $PM_{2.5}$ each year. This has implications for human health because of the fact that the different secondary species can have different adverse health effects as mentioned earlier. For instance, a higher secondary amine contribution to $PM_{2.5}$ in 2006 can increase blot clotting but the presence of more oxidized organics in 2005 would be more likely to cause respiratory problems, if these particles are inhaled and penetrate through the lungs. Schlesinger (2007) stated that since relative toxicity of various constituents of $PM_{2.5}$ probably differs for different observed biological endpoints, the public health risk from each of these components is unlikely to be the same in different geographical regions where the chemical properties of ambient $PM_{2.5}$ may differ (230). Therefore, the same effect would be expected in the same geographic region if the particle chemistry of $PM_{2.5}$ mass is different from year-to-year.

Highly-aged particles accumulate more secondary species which increases toxicity level; hence, it is important to determine the extent of particle aging. The ratio of *m/z*'s 43/37 ($C_2H_3O^+$/$CHNO^+$ to C_3H^+) provides an indication of the extent of particle aging from year-to-year in Riverside. The OC marker *m/z* 37 has been observed as a fresh emission from light duty vehicles (231), while the oxidized OC marker *m/z* 43 signifies a more oxidized/aged species (208). Incorporating O_3 into this ratio can also help determine if the particles were truly aged in the atmosphere. **Figure 50** shows the temporal profile of this ratio as a function of O_3 concentrations. The fact that this ratio is highest during the highest O_3 concentration (13:00-14:00) suggests that particles during this time are more aged with oxidized organics, potentially from oxidized organic gases that condense onto particles or heterogeneous reactions, versus being primary. This trend is similar to what has been previously observed in Riverside with aerosol mass spectrometry (214) and $PM_{2.5}$ filter measurements(232), where semi-volatile organics increased during high mid-day photochemical activity and decreased at night. Even though the relationship between 43/37 and O_3 exists all three years, the diurnal profiles tend to become more variable from 2005-2007 similar to $PM_{2.5}$, where the temporal profiles of $PM_{2.5}$ became less diurnal from 2005-2007 because of the WS and AMBTs becoming less diurnal.

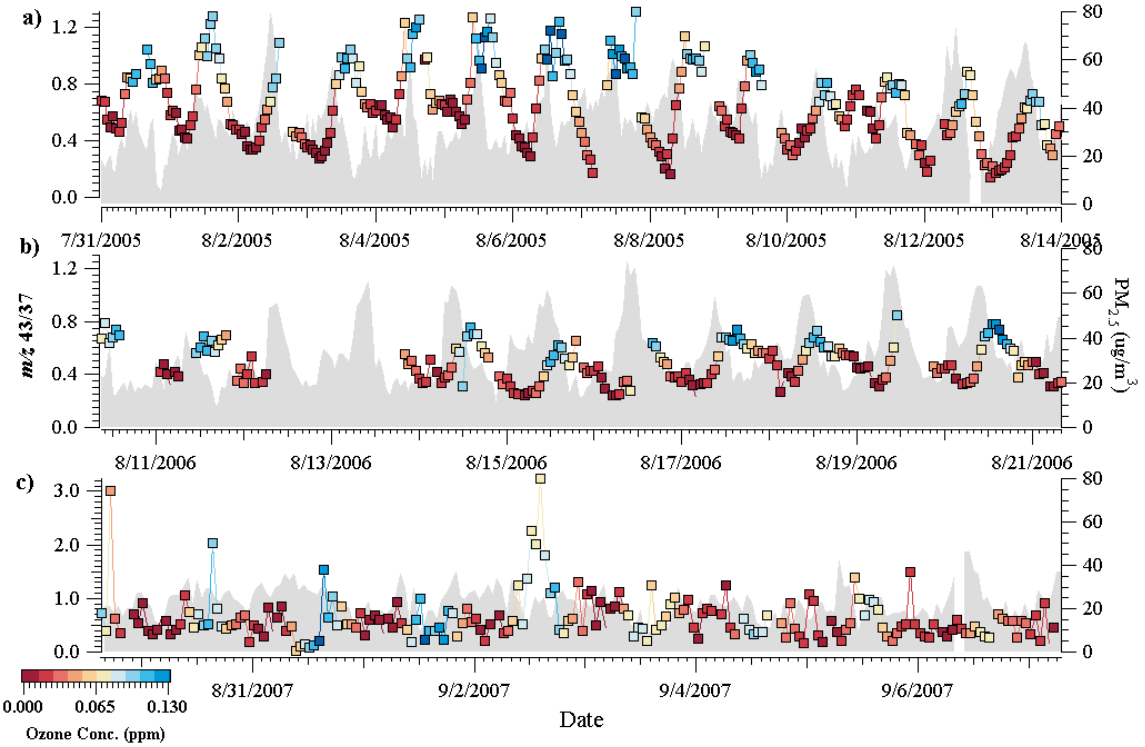

Figure 50: shows the ratio of the sum of peak areas m/z 43 to m/z 37 plotted as a function of O_3 concentration (ppm) from a) 2005, b) 2006, and c) 2007 with maroon being the lowest concentration and blue being the highest. Also pictured is the temporal profile of $PM_{2.5}$ mass concentrations ($\mu g/m^3$).

d. Relating particle chemistry to meteorology and $PM_{2.5}$ mass concentrations

In order to assess the $PM_{2.5}$ trends and relate them to particle chemistry, an overall look at the particle chemistry is required. **Figure 50** illustrates the time-resolved

chemistry of the number fractions of each particle type relative to the total number of particles, which show large variations in particle chemistry between the three summers. Even though organic-containing particles (AgedOC, ECOC, amines, and biomass types combined) comprise the largest number fraction each year (57-86%) for particles 0.2-1.0 um, there are notable differences in the overall particle chemistry which can be tied to gas-phase concentrations and/or meteorology. 2005 had the highest number fraction of AgedOC particles (27%) compared to 2006 (8%) and 2007 (6%). This is likely because of the higher average O_3 concentrations (46.4 ppb) than 2006 (38.8 ppb) or 2007 (39.5 ppb), which would lead to the presence of more oxidized organics. The average RH was highest in 2006 (75%) as was the amine fraction (86% of the total number of particles), compared to 2005 and 2007 (1% and 5% of the total, respectively). Amine particle markers have been previously reported to increase at higher RH and lower T at an urban site (39), suggesting they are semi-volatile and partition to the particle phase under these conditions. In 2007 although the highest relative number fraction of particles was ECOC, there were larger fractions of AgedSS and dust (23% and 10% of the total, respectively) compared to 2005 (20% and 2%) and 2006 (1% and 0.1%), which can be attributed to Santa Anas during the study that transported more dust. The presence of more AgedSS types can be attributed to AMBTs originating over the Pacific Ocean as seen in **Figure 48**. During this time period, a large increase in the fraction of AgedSS is observed in **Figure 50**. Directly before and after this time period, AMBTs were more similar to the Coastal or Northeastern Inland trajectories.

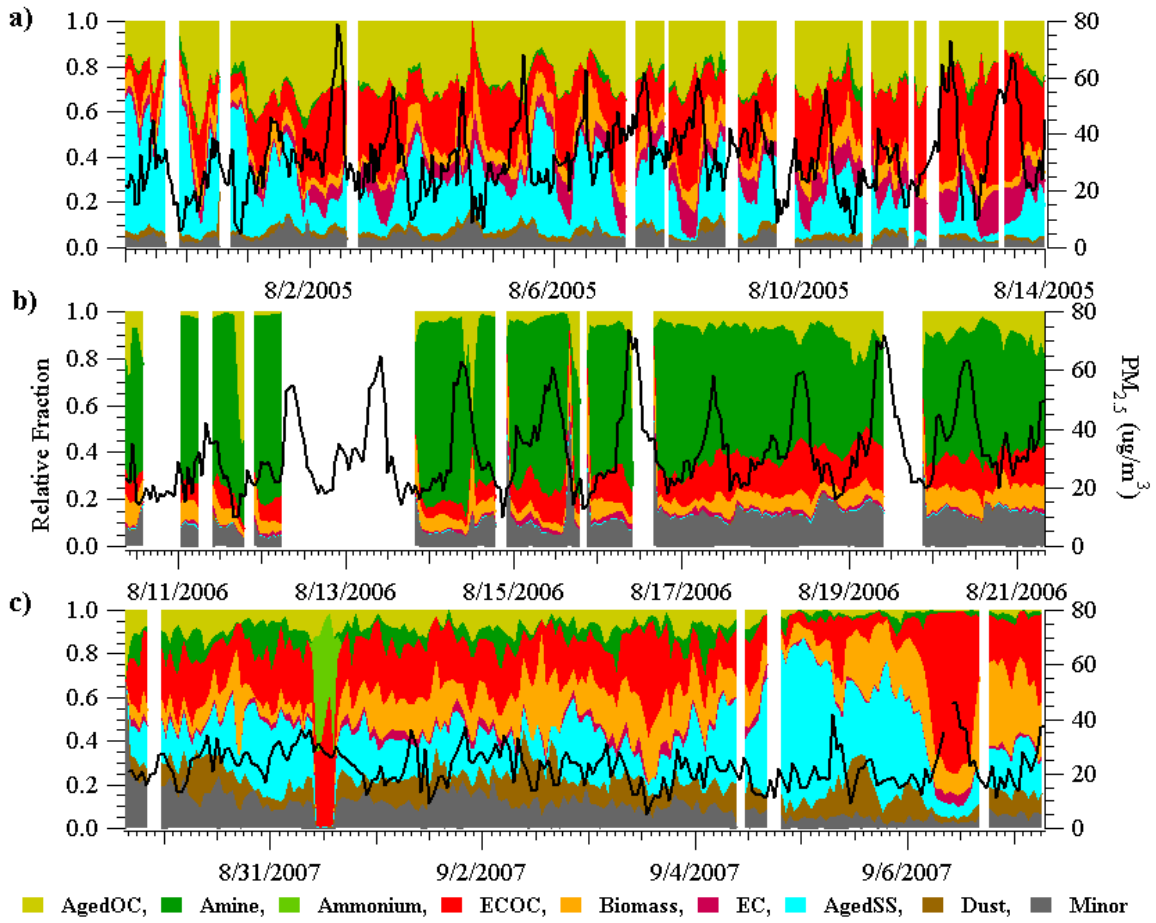

Figure 51: Temporally-resolved submicron particle chemistry from a) 2005, b) 2006, and c) 2007. Hourly $PM_{2.5}$ mass concentrations are also plotted for each year (black line).

The temporal profiles of these particle types also show distinct differences in the relative number fractions due to the diverse meteorology each year (Supplementary Material). However, almost everyday each year a pattern exists between $PM_{2.5}$ and the relative fraction of ECOC particle types, which follow very similar temporal profiles. While organics are linked to respiratory and cardiovascular problems, EC has been shown to cause respiratory problems such as chronic bronchitis, sputum, and coughing (233). The ECOC type is from the aging of EC after it has been emitted from combustion sources. ECOC is also a large number fraction of the total particle counts, equaling 29%, 13%, and 31% in 2005, 2006, and 2007, respectively. **Figure 51** shows temporally-resolved profiles of $PM_{2.5}$ mass concentrations and relative number fraction of the ECOC-type particles. In 2005 and 2007, these fractions are the highest of all particle types and in 2006 the fraction is the second highest after amines. Because ECOC largely contributes to particle number each year, this could be why it greatly influences $PM_{2.5}$ concentrations. There are days where this pattern does not exist, predominantly in 2007. This could be due to the particles from Santa Ana influences, increasing the dust fraction which contributes to the mass instead, such as on August 3, 2007 where ECOC peaks and the $PM_{2.5}$ mass concentrations fall. Also, AgedSS and dust fractions fall during this day,

suggesting that these particle types contribute to mass concentrations more than other types of particles that day.

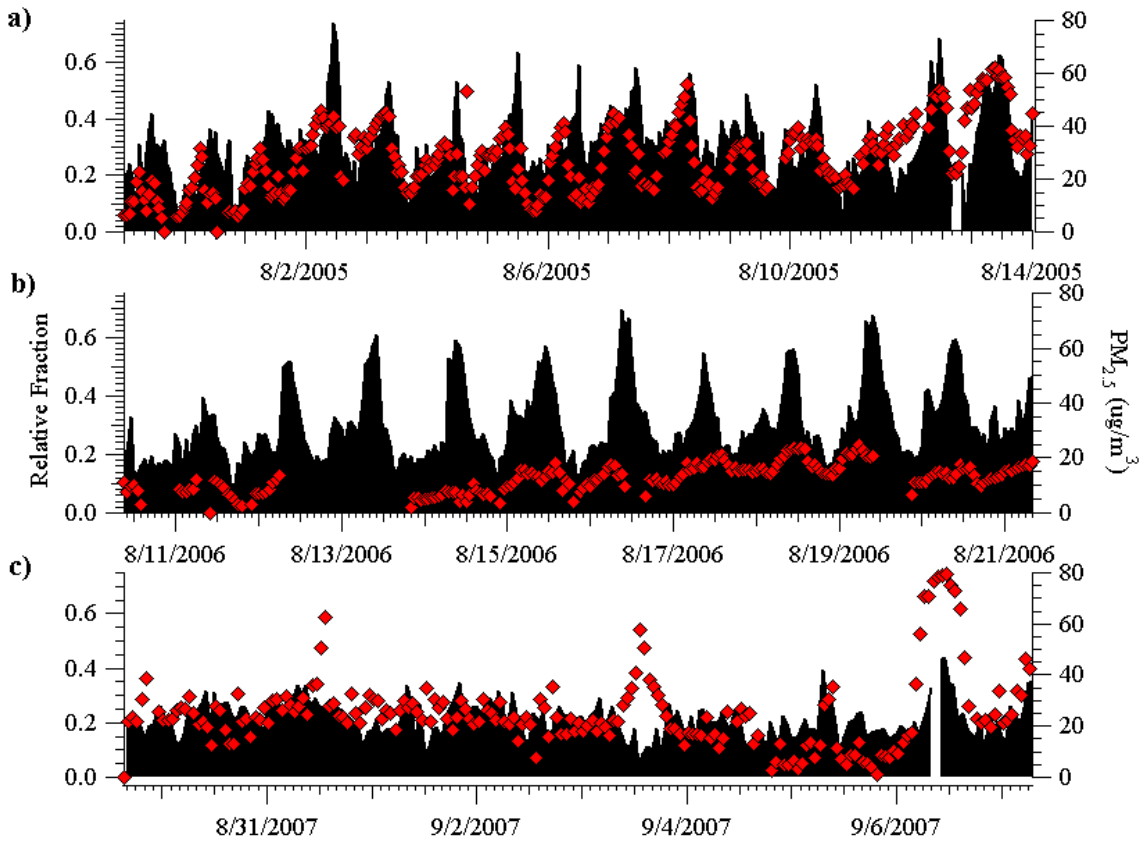

Figure 52: Temporally-resolved relative number fraction of ECOC particle types (red diamonds) from a) 2005, b) 2006, and c) 2007. The black shaded regions are the $PM_{2.5}$ mass concentrations for each year.

Figure 53 shows the size-resolved submicron particle chemistry in Riverside, CA during the three studies of a) 2005, b) 2006, and c) 2007. Similar to the temporally resolved profiles, 2005 showed more evidence of an aged organic atmosphere over the entire submicron size range with larger fractions of the total number of particles being AgedOC and ECOC types and very little fractions of biomass, amines, and inorganics such as dust and AgedSS. In 2006, the high relative humidity and low temperature atmosphere correlated to the presence of a large fraction of amine-containing particle types over the entire submicron size range, with smaller fractions of AgedOC, ECOC, biomass, and inorganic types. The Santa Ana conditions in 2007 led to an increase in the dust fraction, while AgedSS was also present in a high fraction. Organic types (AgedOC, ECOC, biomass, and amines) were smaller fractions than the previous years. Dust was present over the entire size range, while AgedSS was predominant at larger sizes (> 600 nm).

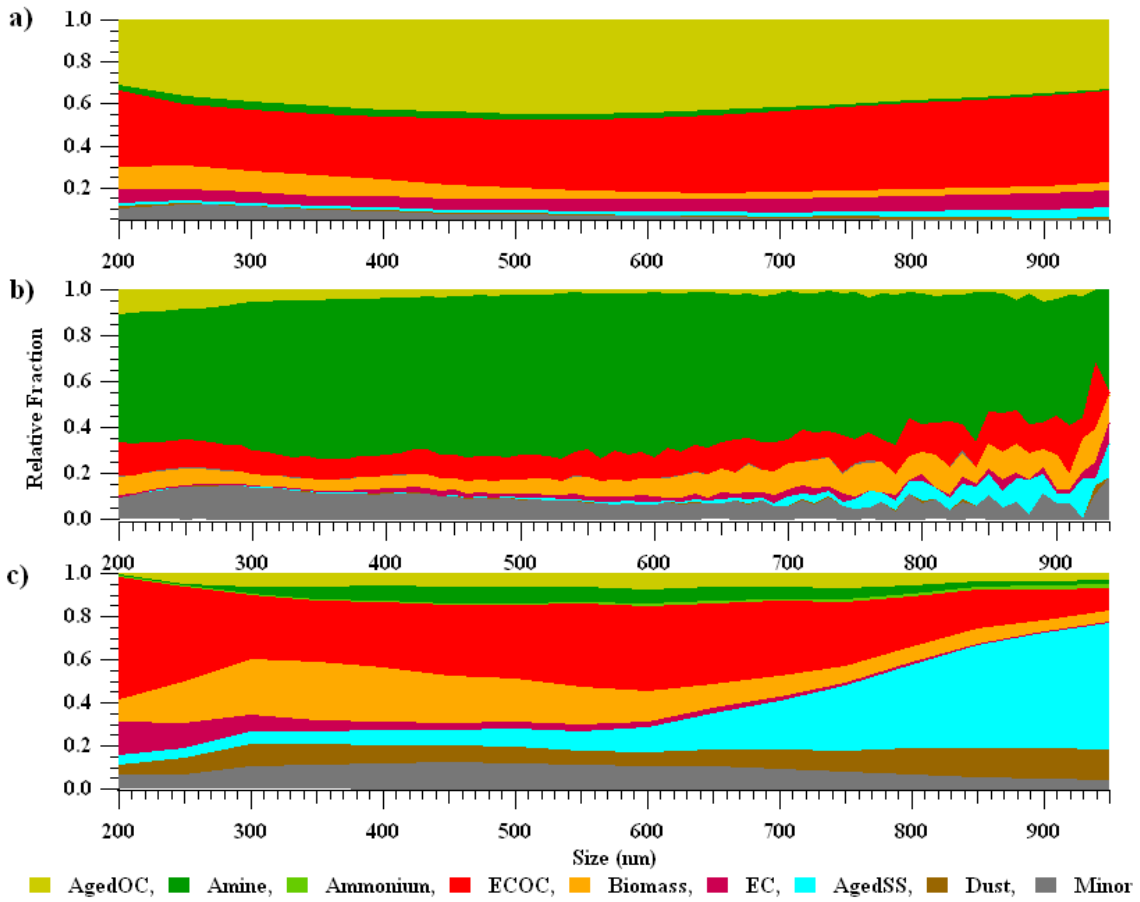

Figure 53: Size resolved submicron particle chemistry in Riverside, CA.

Although inter-annual similarities exist with the relationship between ECOC and $PM_{2.5}$ mass concentrations, the aging of the ECOC types differ each year as seen in **Figure 49**, meaning these particles could have different physical properties, levels of toxicity, and health effects. As mentioned throughout this manuscript, 2005 was a highly-aged atmosphere because of high O_3 levels, while 2006 contained an amine-rich environment because of high RH, and 2007 was highly variable with high T because of Santa Anas. This points out that diverse agconditions affect differences in ECOC each year: 2005 ECOC types were mostly aged with oxidized OC (88% of the total ECOC-type particles), 2006 ECOC were mostly aged with secondary amines (87% of the total ECOC-type particles), while in 2007 ECOC types were mainly aged with nitrate (39% of the total ECOC-type particles). Also, along with $PM_{2.5}$ as discussed earlier, the temporal profiles of ECOC become less diurnal because the WS became less diurnal.

iv. Conclusions

Using ATOFMS, ambient submicron single-particle chemical composition was examined in Riverside, CA over the course of three summers from 2005-2007. Meteorological factors such as T, RH, WS, and O_3 concentrations affected overall particle chemistry and thus $PM_{2.5}$ mass concentrations. In 2005, diurnal profiles of the WS and AMBTs from similar sources led to a very consistent, diurnal profile in $PM_{2.5}$.

O_3 levels were highest in 2005, leading to more aged organic species. 2006 was the moistest year with the lowest average T, leading to more amines versus 2005 and 2007. Santa Anas in 2007 led to high average T and inconsistent WS and AMBTs, which also caused variation in the particle chemistry and $PM_{2.5}$ mass concentrations due to transport from different sources. Besides aging with nitrate each year, particle mixing states were extremely different, with 2005 and 2006 having a higher fraction of organic-containing particles (AgedOC and amines, respectively) aged with secondary species and 2007 having larger fractions of AgedSS and dust aged with secondary species, although organic-containing particles were still highly aged. It is important to consider number and relative amount of secondary species in single-particle mixing states because it can lead to more specific insight on source, on how a particle is altered after emission into the atmosphere, and what sort of adverse health effects are associated with it.

The major particle types varied all three years as shown by the time-resolved chemistry, but evident each year was a similar temporal pattern between the fraction of ECOC-type particles and $PM_{2.5}$ mass concentrations. This suggests that ECOC types are a large contributor to particulate mass concentrations and inhaling these particles can cause acute and chronic respiratory problems. However, this pattern does not exist everyday, meaning other species still contribute to mass and are important to consider.

In general, it cannot be assumed that particle chemistry only seasonally fluctuates with similar particle mixing states and concentrations every year. Variation in particle quantity ($PM_{2.5}$ mass concentrations) and quality (chemical mixing state) exists due to differences in meteorology on top of emissions from different sources year-to-year. Looking at single-particle mixing state can provide more detailed information on what types of particles are contributing to $PM_{2.5}$. However, understanding how a single particle can chemically change with meteorology cannot be based on one major study to represent all years, particularly in a model that relates $PM_{2.5}$ concentrations with adverse health effects such as generalized additive models. Evident from these three studies, each year has very different meteorology which could be used to optimize parameters in health models and therefore improve pollution regulations. Since continuous intensive particle measurements are difficult long-term, the optimized parameters can be used in models to predict how $PM_{2.5}$ changes and what implications it would have on health during a specific type of meteorological condition. In the future, these results could be used as a first approximation as to what the detailed chemical composition of $PM_{2.5}$ may be and therefore generate stricter pollution regulations based on better-defined health effects models.

v. Acknowledgements

We acknowledge Prof. Paul Ziemann (UCR), the UCR Air Pollution Research Center, and the Prather group, particularly Laura Shields and Hiroshi Furutani for support during SOAR. We thank Megan McKay and the Goldstein group (UC-Berkeley) for the meteorological measurements in 2005. Air mass back trajectories were produced with the Hybrid Single-Particle Lagrangian Integrated Trajectory model (NOAA). This work was supported by the California Air Resources Board (CARB 04-336) and the National Science Foundation (NSF ATM-0321362). K. Pratt has been supported by a NSF Graduate Research Fellowship and in part by an EPA STAR Graduate Fellowship (2006-

2009); the EPA has not officially endorsed this publication, and the views expressed herein may not reflect the views of the EPA.